Ru^{II} Complexes Incorporating Tetrathiamacrocycles: Synthesis and Conformational Analysis

Harry Adams,[a] A. M. Amado,[b] Vitor Félix,*[b] Brian E. Mann,*[a] Jorge Antelo-Martinez,[a] Mike Newell,[a] Paulo J. A. Ribeiro-Claro,[b] Sharon E. Spey,[a] and James A. Thomas*[a]

Abstract: The synthesis of a series of Ru^{II} complexes incorporating thiacrown ligands ([12]ane-S_4, [14]ane-S_4, [16]ane-S_4), as well as 2,2′-bipyridine (bpy) or pyridine, is reported. Structural studies on these complexes have been carried out using a variety of techniques. Detailed ^{1}H NMR spectroscopic studies on the previously reported $[Ru([12]ane\text{-}S_4)(bpy)]^{2+}$ (**1**) reveal that—contrary to earlier reports—the observed fluxional ^{1}H NMR behavior is not due to chemical exchange involving cleavage of the bpy Ru–N bond but is, in fact, due to lone-pair inversion of coordinated macrocyclic sulfur donor atoms. This phenomenon is also observed for the [14]ane-S_4 and [16]ane-S_4 analogues of **1**. For the first time, using a combination of X-ray crystallography, more detailed ^{1}H NMR experiments, and computational methods, an in-depth study on the energetics and dynamics of invertomer formation and conversion for macrocyclic coordination complexes has been carried out. These studies reveal that the steric constraints of assembling each sulfur macrocycle and bpy ligand around the octahedral Ru^{II} center lead to close intramolecular contacts. These contacts are largely dependent on the orientation of the electron lone pairs of equatorial sulfur donor atoms and correlate with the comparative stability of the different invertomeric forms. Thus, the conformational preferences of the three macrocyles in $[Ru([n]ane\text{-}S_4)(bpy)]^{2+}$ complexes are determined by steric rather than electronic effects.

Keywords: fluxionality · invertomers · macrocylic ligands · ruthenium · sulfur

Introduction

The observation of intervalence charge transfer in the Creutz–Taube ion[1] has led to $Ru^{II/III}$ complexes playing a key part in the investigation of electron-transfer processes.[2,3] Consequently, mixed-valence bimetallic complexes incorporating metal centers, such as $[Ru(bpy)_2]^{2+}$ and $[Ru(NH_4)_5]^{2+}$ (bpy = 2,2′-bipyridine), have played an important role in the development of devices for molecular electronics.[4] Virtually all this research has involved nitrogen-based auxillary ligands, such as NH_3 and bpy, coordinated to the metal ion. We have been broadening the experimental basis of such work by introducing new metal complexes containing sulfur-donor macrocyclic ligands. The first steps in such work have focused on the readily available thio macrocycle [9]ane-S_3.[5] Previously, the fragment $[Ru([9]ane\text{-}S_3)]^{2+}$ has been used to construct electron-transfer systems and supramolecular architectures.[6–8] As part of a long-term aim to create molecular devices with targeted coordination geometries, we are now investigating the chemistry of related $[Ru([n]ane\text{-}S_4)]^{2+}$ metal centers.

Previous reports have demonstrated that $[Ru(dmso)Cl(L^1)]^+$ (L^1 = [12]ane-S_4, dmso = dimethyl sulfoxide) is a suitable starting material for the preparation of bidentate polypyridyl complexes incorporating $[Ru(L^1)]$ metal centers, such as $[Ru(L^1)(phen)](PF_6)_2$ (phen = 1,10-phenanthroline) and **1**-$(PF_6)_2$.[9] Crystallographic data showed that in order to accommodate the relatively small cavity of the coordinated L^1 ring and bite angle of the pyridyl ligand, the coordination geometry around the Ru^{II} ion was distorted away from octahedral symmetry. Furthermore, such complexes displayed fluxional ^{1}H NMR behavior, with the signals for coordinated

[a] H. Adams, Prof. B. E. Mann, J. Antelo-Martinez, M. Newell, S. E. Spey, Dr. J. A. Thomas
Department of Chemistry, University of Sheffield
Sheffield, S3 7HF (UK)
Fax: (+44) 114-222-9346
E-mail: b.mann@sheffield.ac.uk
james.thomas@sheffield.ac.uk

[b] A. M. Amado, Prof. V. Félix, P. J. A. Ribeiro-Claro
Departamento de Química, CICECO, Universidade de Aveiro
3810–193 Aveiro (Portugal)
Fax: (+351) 234-370-084
E-mail: vfelix@dq.ua.pt

 DOI: 10.1002/chem.200400693

aromatic protons and the CH_2 units of [12]ane-S_4 being broad.[9a] It was suggested that these observations were due to chemical exchange involving cleavage of the Ru–N bond, relieving the distortion observed in the solid state.

It is well established that higher tetrathiamacrocycles, which possess larger cavity sizes, such as [14]ane-S_4 (L^2) and [16]ane-S_4 (L^3), are more accommodating in terms of their coordination geometry; for example, while $[RhCl_2L^1]$ and $[RhCl_2L^2]$ are isolated as *cis* isomers, $[RhCl_2L^3]$ is obtained as a *trans* isomer.[10] Therefore, with the aim of synthesizing suitable, nonfluxional building blocks for the construction of oligomeric complexes, he substitution chemistry of $[Ru(L^1)]$, $[Ru(L^2)]$ and $[Ru(L^3)]$ metal centers with pyridine (py) and bpy was investigated.

Table 1. Summary of crystallographic data for **3** and **6**.

	4-$(PF_6)_2$[a]	**5**-$(PF_6)_2$[b]	**6**-$(PF_6)_2$[c]
formula	$C_{20}H_{28}F_{12}N_2P_2RuS_4$	$C_{22}H_{32}F_{12}N_2P_2RuS_4$	$C_{21}H_{32}F_{12}N_2OP_2RuS_4$
M_r	815.69	843.75	847.74
crystal system	monoclinic	monoclinic	monoclinic
space group	$P2_1/n$	$P2_1/c$	$P2_1/c$
crystal size [mm^{-1}]	$0.31\times0.21\times0.19$	$0.35\times0.26\times0.21$	$0.21\times0.12\times0.08$
a [$Å^{-1}$]	12.1828(10)	17.4077(16),	18.4021(13)
b [$Å^{-1}$]	11.8928(9)	11.8261(11),	10.6165(7)
c [$Å^{-1}$]	22.4693(18)	17.0058(16)	15.9240(11)
β [°]	103.4780(10)	110.407(2)	97.1660(10)
V [$Å^{-3}$]	3165.9(4)	3281.2(5)	3086.7(4)
Z	4	4	4
ρ_{calcd} [$Mg\,m^{-3}$]	1.711	1.708	1.824
$F(000)$	1632	1696	1704
$\mu(Mo_{K\alpha})$ [mm^{-1}]	0.947	0.917	0.977
final R_1 (on F)	0.0446	0.0485	0.0499
final wR_2 (on F)[a–c]	0.1142	0.1243	0.0981

[a] A weighting scheme, $w=1/[\sigma^2(F_o^2)+(0.0570P)^2+2.8368P]$ in which $P=(F_o^2+2F_c^2)/3$, was used in the latter stages of refinement. [b] A weighting scheme, $w=1/[\sigma^2(F_o^2)+(0.0628P)^2+0.00P]$ in which $P=(F_o^2+2F_c^2)/3$, was used in the latter stages of refinement. [c] A weighting scheme, $w=1/[\sigma^2(F_o^2)+(0.0503P)^2+0.00P]$ in which $P=(F_o^2+2F_c^2)/3$, was used in the latter stages of refinement.

Results and Discussion

Synthetic and structural details: Addition of Ag^+ ions to starting materials **2** and **3** followed by the addition of bpy

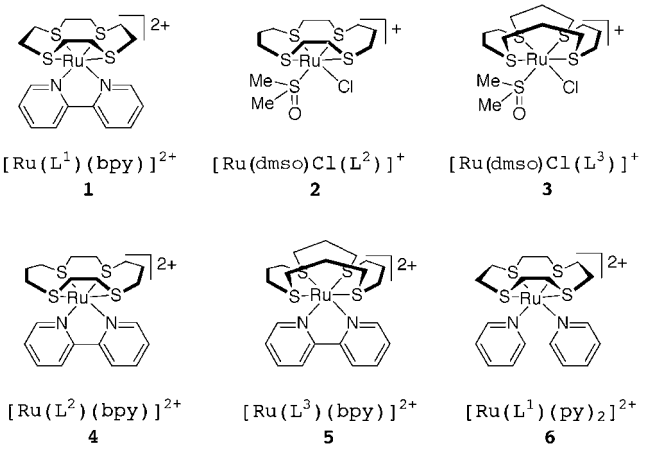

led to the isolation of **4** and **5**, respectively, as analytically pure hexafluorophosphate salts. In a similar manner, the bis-substituted complex **6** was obtained when a solution of $[Ru(dmso)Cl(L^1)]PF_6$ was first treated with Ag^+ followed by the addition of excess pyridine. Again, **6** was isolated in good yields as a analytically pure hexafluorophosphate salt without further work up. The solid-state structures of all three products were confirmed by X-ray crystallography (see Table 1). The crystallographic data offers an informative comparison between the coordination demands of L^1, L^2, and L^3.

The previously reported structure of **1** shows a large distortion from idealized octahedral geometry; for example, the angle between the two axial sulfur donor atoms and the Ru ion, S_{ax}-Ru-S_{ax}, is 162.5(2)°, whereas the S_{eq}-Ru-S_{eq} angle between two equatorial sulfur donor atoms and the Ru ion is distorted away from the idealized 90°, being instead 104.5(1)°. The corresponding angles in **4** are 177.21(4)° for S_{ax}-Ru-S_{ax} and 87.90(3)° for S_{eq}-Ru-S_{eq} (Figure 1, Table 2).

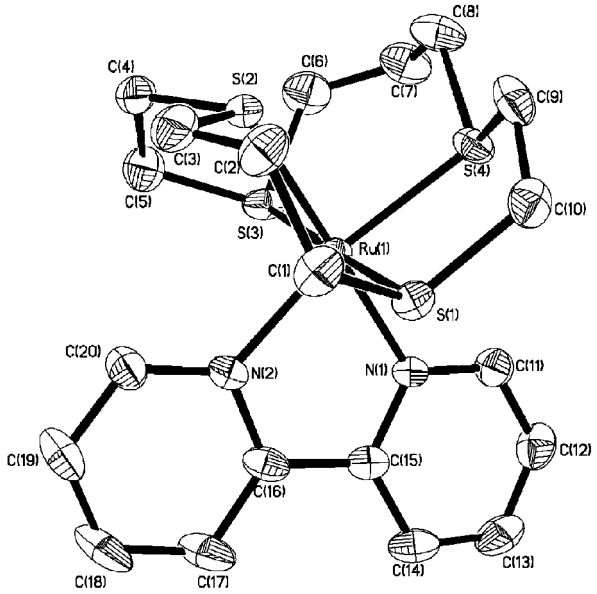

Figure 1. ORTEP plot of the cation in **4**-$(PF_6)_2$. Hydrogen atoms are removed for clarity.

However, while the S_{eq}-Ru-S_{eq} angle for **5** is 88.26(4)°, the S_{ax}-Ru-S_{ax} angle opens out slightly to 187.99(6)° (Figure 2, Table 3). A comparison of S_{eq}-Ru-N bond angles also indi-

Table 2. Selected bond lengths [Å] and angles [°] for complexes **4**-$(PF_6)_2$.

Bond lengths		Bond angles	
Ru–N(1)	2.109(3)	N(1)-Ru-N(2)	77.39(11)
Ru–N(2)	2.119(3)	N(1)-Ru-S(1)	88.43(8)
Ru–S(1)	2.3403(9)	N(1)-Ru-S(2)	178.32(8)
Ru–S(2)	2.3171(9)	N(1)-Ru-S(3)	94.36(8)
Ru–S(3)	2.3558(10)	N(1)-Ru-S(4)	92.98(8)
Ru–S(4)	2.3131(10)	N(2)-Ru-S(1)	89.35(9)
		N(2)-Ru-S(2)	101.86(9)
		N(2)-Ru-S(3)	91.05(9)
		N(2)-Ru-S(4)	190.76(1)
		S(1)-Ru-S(2)	93.07(3)
		S(1)-Ru-S(3)	177.21(4)
		S(1)-Ru-S(4)	85.54(3)
		S(2)-Ru-S(3)	84.14(4)
		S(2)-Ru-S(4)	87.90(3)
		S(3)-Ru-N(4)	94.52(4)

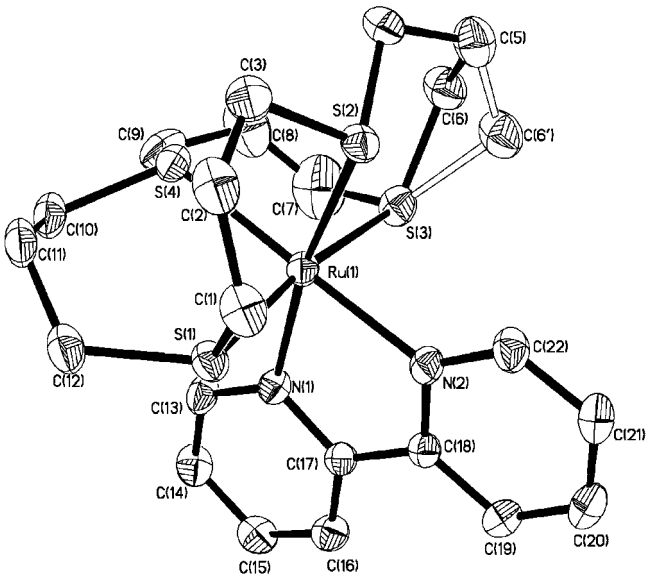

Figure 2. ORTEP plot of the cation in **5**-$(PF_6)_2$ showing modeling of disordered coordinated thiacrown ligand. Hydrogen atoms are removed for clarity.

Table 3. Selected bond lengths [Å] and angles [°] for complexes **5**-$(PF_6)_2$.

Bond lengths		Bond angles	
Ru–N(1)	2.111(3)	N(1)-Ru-N(2)	78.14(13)
Ru–N(2)	2.114(3)	N(1)-Ru-S(1)	87.23(9)
Ru–S(1)	2.3595(11)	N(1)-Ru-S(2)	190.10(9)
Ru–S(2)	2.3415(10)	N(1)-Ru-S(3)	172.00(4)
Ru–S(3)	2.3533(11)	N(1)-Ru-S(4)	101.71(9)
Ru–S(4)	2.3376(11)	N(2)-Ru-S(1)	86.74(9)
		N(2)-Ru-S(2)	91.95(10)
		N(2)-Ru-S(3)	85.95(9)
		N(2)-Ru-S(4)	178.06(9)
		S(1)-Ru-S(2)	90.25(4)
		S(1)-Ru-S(3)	187.99(6)
		S(1)-Ru-S(4)	95.19(4)
		S(2)-Ru-S(3)	93.26(4)
		S(2)-Ru-S(4)	88.26(4)
		S(3)-Ru-N(4)	92.11(4)

cates that **4** and **5** are less distorted: in **1**, both S_{eq}-Ru-N_{trans} = 166.7°, while for **4**, S_{eq}-Ru-N_{trans} = 178.32(8) and 190.76(1)°, and for **5**, S_{eq}-Ru-N_{trans} = 178.06(9) and 190.10(9)°. The small cavity size of L^1 within the $\mathbf{1}^{2+}$ cation also results in a difference in axial Ru–S_{ax} and equatorial Ru–S_{eq} bond lengths, with the former being significantly longer (> 0.1 Å) than the latter. The structures of **4** and **5** display a similar trend, but to a much smaller degree: for **4**, Ru–S_{ax} = 2.3403(9) and 2.3558(10) Å compared with Ru–S_{eq} = 2.3171(9) and 2.3131(10) Å, while for **5**, Ru–S_{ax} = 2.3595(11) and 2.3533(11) Å compared with Ru–S_{eq} = 2.3415(10) and 2.3376(11) Å.

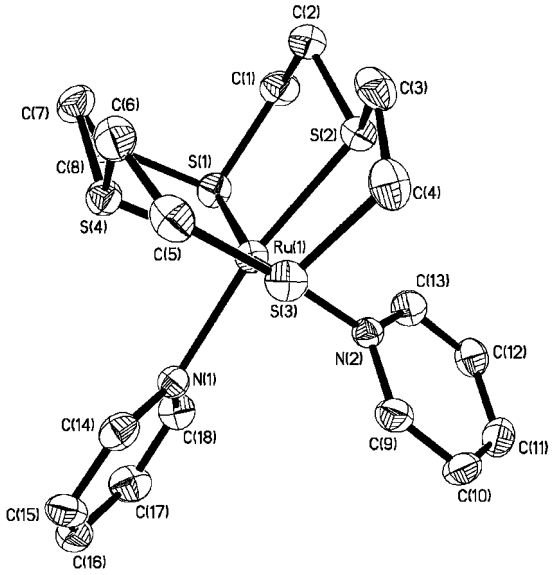

Figure 3. ORTEP plot of the cation in **6**-$(PF_6)_2$. Hydrogen atoms are removed for clarity.

The structure of complex **6**, shown in Figure 3, is less distorted away from model octahedral geometry than **1**, as the non-chelating monodentate ligands allow the N-Ru-N bond angle (85.52(13)°) to take a value closer to the idealized 90°. However, the structural demand produced by the small cavity size of L^1 still produces distinct effects. For example, S_{ax}-Ru-S_{ax} is 161.78(4)°, whereas S_{eq}-Ru-S_{eq} is 106.66(4)°, and the average Ru–S_{ax} bond length is 2.3796(62) Å, while the corresponding Ru–S_{eq} bond length is almost exactly 2.30 Å. See Table 4 for more details on relevant bond lengths and angles.

^{1}H NMR studies: Despite the crystallographic evidence that the Ru coordination spheres of **4** and **5** are much less distorted than that of **1**, somewhat surprisingly, both new complexes also display fluxional ^{1}H NMR behavior, vide infra, suggesting that the previously postulated chemical exchange mechanism is incorrect. This prompted us to re-examine the ^{1}H NMR properties of **1** in more detail and at a lower temperature than the previously reported studies.[9]

Table 4. Selected bond lengths [Å] and angles [°] for complexes **6**-$(PF_6)_2$.

Bond lengths		Bond angles	
Ru–N(1)	2.156(3)	N(1)-Ru-N(2)	85.52(13)
Ru–N(2)	2.130(3)	N(1)-Ru-S(1)	95.03(10)
Ru–S(1)	2.3748(12)	N(1)-Ru-S(2)	169.36(10)
Ru–S(2)	2.2996(12)	N(1)-Ru-S(3)	98.54(10)
Ru–S(3)	2.3845(12)	N(1)-Ru-S(4)	83.76(10)
Ru–S(4)	2.3003(12)	N(2)-Ru-S(1)	97.61(10)
		N(2)-Ru-S(2)	84.11(10)
		N(2)-Ru-S(3)	95.52(10)
		N(2)-Ru-S(4)	169.18(10)
		S(1)-Ru-S(2)	84.00(4)
		S(1)-Ru-S(3)	161.78(4)
		S(1)-Ru-S(4)	84.80(4)
		S(2)-Ru-S(3)	84.86(4)
		S(2)-Ru-S(4)	106.66(4)
		S(3)-Ru-N(4)	84.65(4)

At room temperature, the ^{1}H NMR spectrum of **1**-$(PF_6)_2$ in [D_6]acetone does show one set of broadened signals. However, on cooling to −43 °C, the signals split to give two sets of signals, see Figure 4. The two isomers are present in a ratio of 1.00:0.16. This corresponds to a ΔG°_{230} of 3.5 kJ mol^{-1}.

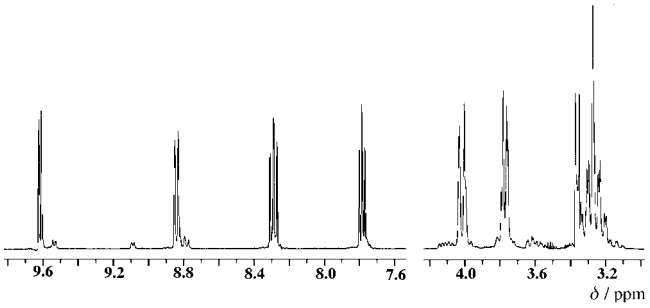

Figure 4. The 400 MHz ^{1}H NMR spectrum of **1**-$(PF_6)_2$ in [D_6]acetone at −43 °C.

Three possible isomers can arise from the orientation of the macrocyclic sulfur lone pairs: **1a**, **1b**, and **1c**. Ligand

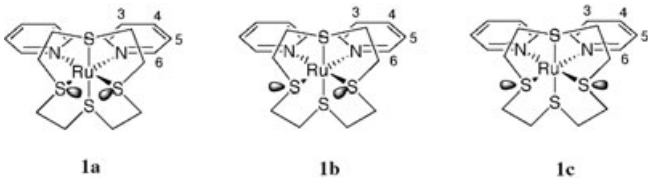

conformation **1c** is found in the crystal structures of **1**-Cl_2, [Ru(L^1)(phen)]Cl_2, and [Ru(L^1)(4,7-Ph_2-phen)]Cl_2 (Ph = phenyl, phen = 1,10-phenanthroline),[9] and also **6**-$(PF_6)_2$. While the ligand conformation of **1b** is found in the crystal structures of cations such as [$Ni_2(L^1)_2(\mu$-$Cl)_2$]$(BF_4)_2$[17] and [Rh(L^1)(phi)]Br_3[18] (phi = 9,10-phenanthrene-quinone diimine). As far as we are aware, isomer **1a** has not been observed crystallographically.

From the ^{1}H NMR spectrum, it is clear that the major isomer in solution is symmetric with only one set of four signals for the bpy ring and one set of four signals for L^1. This is consistent with the C_{2v} symmetry of **1a** or **1c**. Since structure **1a** has not been reported in crystal structure analyses, and the solid-state structure of **1** is **1c**, it seems likely that the major isomer in solution is also **1c**.

The ^{1}H NMR signals of the minor isomer are partially obscured by the signals corresponding to the major isomer—the signals were partially assigned using COSY-45 and exchange spectroscopy (EXSY; see Figures 5 and 6). In the

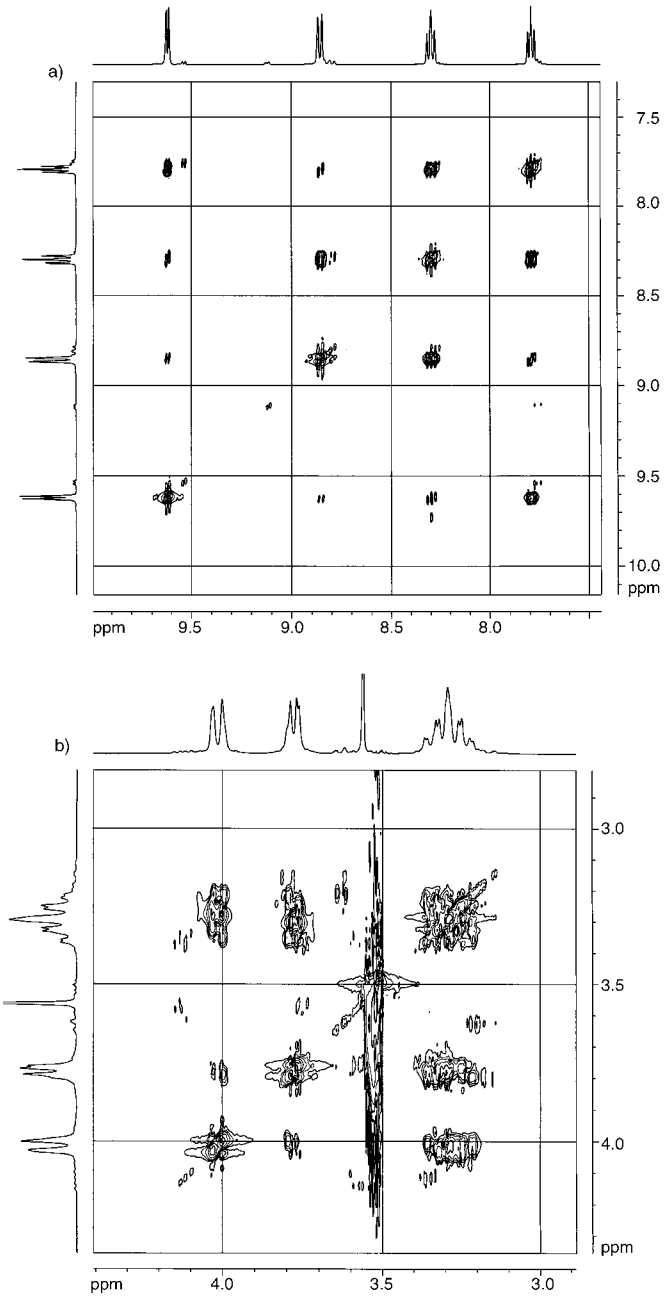

Figure 5. The 400 MHz COSY-45 ^{1}H NMR spectrum of **1**-$(PF_6)_2$ in [D_6]acetone at −43 °C: a) aromatic signals; b) thiacrown signals.

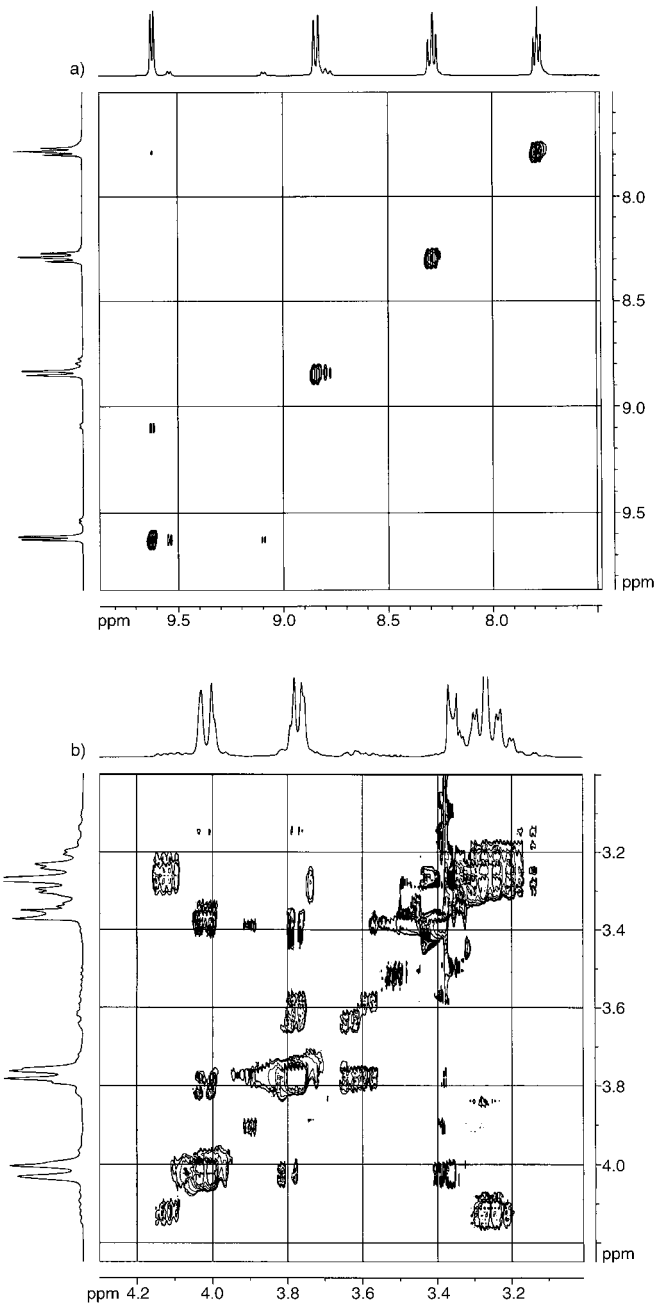

Figure 6. The 400 MHz EXSY ^{1}H NMR spectrum of **1**-$(PF_6)_2$ in [D_6]acetone at −43 °C with a mixing time of 0.5 s and a relaxation delay of 0.5 s: a) aromatic signals; b) thiacrown signals.

COSY-45 spectrum, the connectivity through the negative ^2J was differentiated from the positive ^3J by the lean of the cross-peaks. The EXSY spectrum was used to partially identify the exchanging sets of L^1 ^{1}H NMR signals.

In the bpy region of the spectrum, the minor isomer has two well-resolved H^6 protons at $\delta =$ 9.09 and 9.54 ppm. Similarly, in the methylene region of the spectrum, the COSY-45 NMR picks out two sets of four protons consistent with two different types of SCH_2CH_2S groups. This is consistent with the C_s symmetry of **1b**. These spectra have led to the assignment of the signals shown in Table 5.

The EXSY spectrum shows exchange between the minor and major isomer, but not direct exchange between the two sets of protons in the minor isomer. This is consistent with a mechanism of exchange between **1b** and **1c** involving inversion at the sulfur atoms. Exchange of the inequivalent bpy protons in **1b** would involve the improbable process of concerted inversion at both sulfur atoms. Analysis of the intensities of the cross peaks at −43 °C gives rates of major to minor isomer conversion of 0.18 s^{-1}, and minor to major of 1.1 s^{-1}. These figures correspond to $\Delta G^{\ddagger}_{230}$(major to minor) = 59 ± 2 and $\Delta G^{\ddagger}_{30}$(minor to major) = 56 ± 2 kJ mol^{-1}.

Examination of the $J_{H,H}$ values has permitted a tentative assignment of the methylene protons. For each CH_2CH_2 group, one CH_2 group has $^2J = 11$ Hz while the other has $^2J = 14$ Hz. Examination of the crystal structures shows that the S_{eq}-C-C angle is around 106°. It is therefore probable that the H-C-H angle at S_{eq}-CH_2-C is greater than 109.5°. Similarly, as the S_{ax}-C-C angle is around 114°, it is thus probable that the H-C-H angle at S_{ax}-CH_2-C is less than 109.5°. It is known that ^2J depends on the H-C-H angle with the magnitude decreasing with increasing angle.[20] Therefore, it is probable that the CH_2 group with $^2J = 11$ Hz is S_{eq}-CH_2, while that with $^2J = 14$ Hz is S_{ax}-CH_2. Using the Karplus relationship, ^3J values can be used to further assign signals. Within each CH_2CH_2 group there is one $^3J = \sim 14$ Hz, implying an approximately 180° torsion angle, as found in the crystal structure.

The above data suggests that the observed fluxionality of **1** is not due to the dissociation of one nitrogen of the bpy ligand, but coordinated sulfur lone-pair inversions, that is interconversion of invertomers. This phenomenon has rarely been discussed in the literature; work by Barton et al. has established that L^1 is exclusively found as the **b** form invertomer in the solid state and solution structure of $[Rh(L^1)(phi)]^{3+}$.[18] While NMR fluxionality in square-planar complexes containing the selenium analogue of L^3 has been ascribed to Se lone-pair inversion,[21] the octahedral complex *trans*-[Ru([16]ane-Se_4)Cl_2]$^+$ is found as only one invertomer.[22]

Table 5. Full assignment of ^{1}H NMR signals for isomers of **1**-$(PF_6)_2$ [δ in ppm, J in Hz].

	Major isomer	Minor isomer
	bpy	bpy
H^3	$\delta = 8.84$, $J_{3,4} = 8.0$;	$\delta = 8.81$, $J_{3,4} = 8.0$; $\delta = 8.78$, $J_{3,4} = 8.0$;
H^4	$\delta = 8.30$, $J_{3,4} = 8.0$, $J_{4,5} = 7.6$, $J_{4,6} = 1.5$;	$\delta = 8.30$, (obscured);
H^5	$\delta = 7.78$, $J_{3,5} = 1.3$, $J_{4,5} = 7.5$, $J_{5,6} = 5.8$;	$\delta = 7.76$, extensive overlap;
H^6	$\delta = 9.64$, $J_{4,6} = 1.2$, $J_{5,6} = 5.9$;	$\delta = 9.54$, $J_{5,6} = 5.9$; $\delta = 9.09$, $J_{5,6} = 5.9$;
	[12]ane-S_4	[12]ane-S_4
CH_2	$\delta = 4.07$, $^2J = 14$, $^3J = 5$; $\delta = 3.25$, $^2J = 14$, $^3J = 14$, 5;	$\delta = 3.97$, (obscured); $\delta = 3.80$, (obscured);
CH_2	$\delta = 3.77$, $^2J = 12$, $^3J = 5$; $\delta = 3.29$, $^2J = 12$, $^3J = 5$, 14	$\delta = 3.63$, $^2J = 11$, $^3J = 3$; $\delta = 3.14$, $^2J = {}^3J = 14$, $^3J = 3$;
CH_2		$\delta = 4.12$, $^2J = 13.5$, $^3J = 8$, 1.5; $\delta = 3.36$, (obscured);
CH_2		$\delta = 3.57$; $\delta = 3.77$ (obscured)

In order to test this theory, the corresponding bis-pyridine complex **6**-$(PF_6)_2$ was studied. At room temperature, the ^{1}H NMR spectrum of **6**-$(PF_6)_2$ in $[D_6]$acetone shows two sets of signals, one due to a symmetric isomer, analogous to **1a** or **1c**, and an asymmetric isomer, analogous to **1b**, in the ratio 1:1.9. On the basis of the arguments already presented for **1**, it is probable that the symmetric isomer has a conformation that is analogous to **1c**, which is observed in the solid-state structure. Signals were assigned by using COSY-45 and phase-sensitive NOESY spectroscopy. Broadening due to isomer exchange is noticeable at 37 °C. Pyridine was added to the sample and the integrated ^{1}H NMR spectrum showed a ratio of symmetric isomer/asymmetric isomer/free pyridine of 1.00:2.04:4.19. An EXSY spectrum indicated exchange between the symmetric and asymmetric isomers, but no exchange between the coordinated and free pyridines (Figure 7). A quantitative analysis of the EXSY spectrum yielded a rate of exchange of 6.16 s^{-1} from minor to major isomer and 3.01 s^{-1} from major to minor isomer corresponding to $\Delta G^{\ddagger}_{310}$(major to minor) $= 73 \pm 2$ kJ mol^{-1} and $\Delta G^{\ddagger}_{310}$(minor to major) $= 71 \pm 2$ kJ mol^{-1}. As no exchange was observed with the free pyridine, the mechanism of exchange clearly does not involve pyridine dissociation. This observation further confirms that a ligand dissociation mechanism for the fluxionality in the NMR spectrum of **1**-$(PF_6)_2$ involving chelated bpy is highly unlikely.

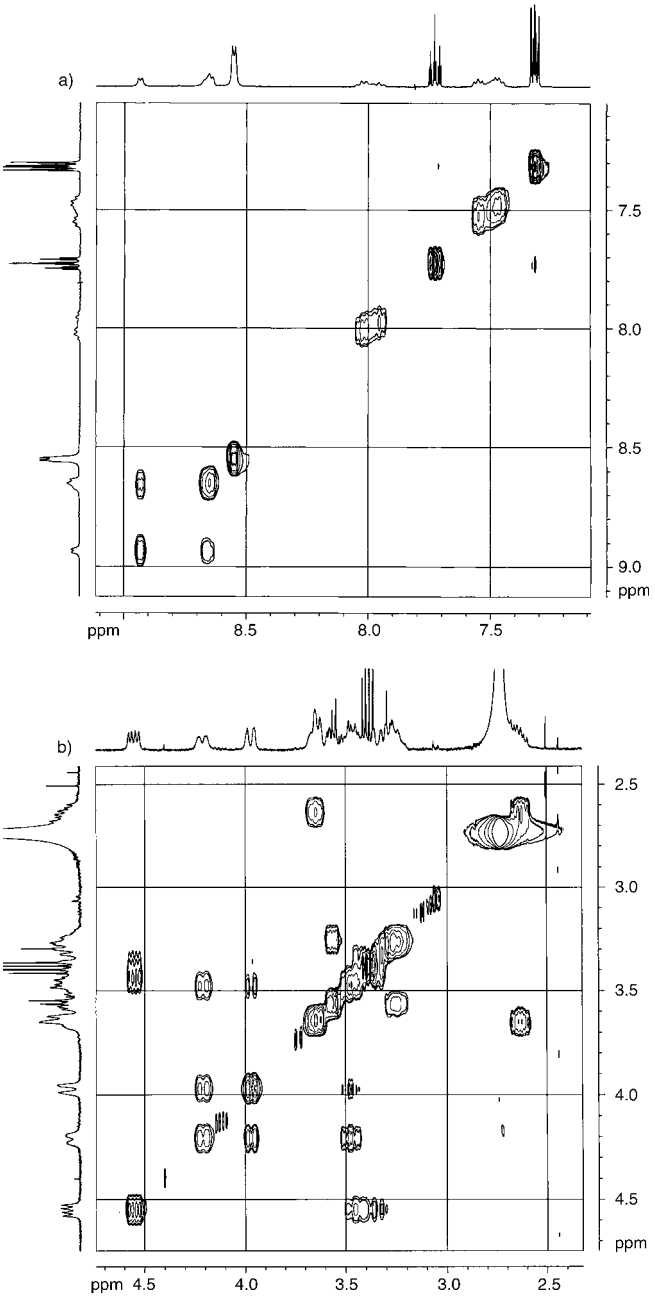

Figure 7. The 400 MHz EXSY ^{1}H NMR spectrum of **6**-$(PF_6)_2$ with the addition of pyridine, in $[D_6]$acetone at 37 °C with a mixing time of 0.1 s and a relaxation delay of 5 s: a) aromatic signals; b) thiacrown signals.

The discovery that ^{1}H NMR line broadening for **1** and **6** is consistent with interconversion of invertomers prompted us to further investigate the ^{1}H NMR properties of **4** and **5**.

The ^{1}H NMR spectrum of **4**-$(PF_6)_2$ in $[D_6]$acetone at room temperature is broadened by exchange. However, on cooling to −15 °C, the signals sharpen. The ^{1}H NMR spectrum is consistent with the presence of one isomer in which all the protons are inequivalent. As with $\mathbf{1}^{2+}$, there are three isomers possible due to sulfur inversion: **4a**, **4b**, and **4c**. The

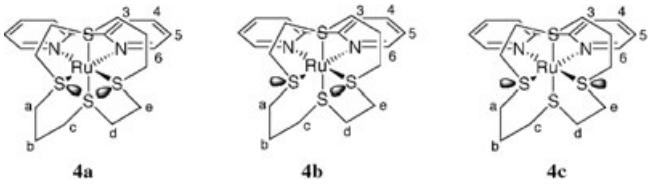

conformation of L^2 in **4a** has been observed in the crystal structures of $[Cr(L^2)Cl_2]PF_6$,[23] $[Ru(L^2)Cl_2]$, $[Ru(L^2)py_2](PF_6)_2$,[24] and $[\{Ni(L^2)\}_2(\mu\text{-}Cl)_2](BF_4)_2$.[17] The conformation of L^2 in **4b** has been observed in the crystal structures of $[Ru(L^2)Cl(PPh_3)]^+$,[25] $[Ir(L^2)Cl_2]BPh_4$,[26] and $[Hg(L^2)(picrate)_2]$.[27] The conformation of L^2 shown in **4c** does not appear to have been observed crystallographically.

In principle, further isomers are possible due to the conformation of the six-membered $[CH_2(CH_2S)_2Ru]$ rings, but as no evidence was found for this extra complication, it will not be considered further for this complex—although it will prove to be significant for the L^3 complex, vide infra. In order to assist the assignment of the ^{1}H NMR spectrum, the COSY-45 NMR spectrum was also recorded at −15 °C, see Figure 8. The spectrum showed the presence of 28 inequivalent protons in equal intensities. This is consistent with **4b** being the only species present; it is viewed as being highly unlikely that **4a** and **4c** are present in equal concentrations without any **4b** being present. These studies confirm that the isomer found in the crystal structure of **4**-$(PF_6)_2$ is also the exclusive solution structure.

The EXSY spectrum at room temperature clearly demonstrated pairwise exchange of the protons (Figure 9). The ob-

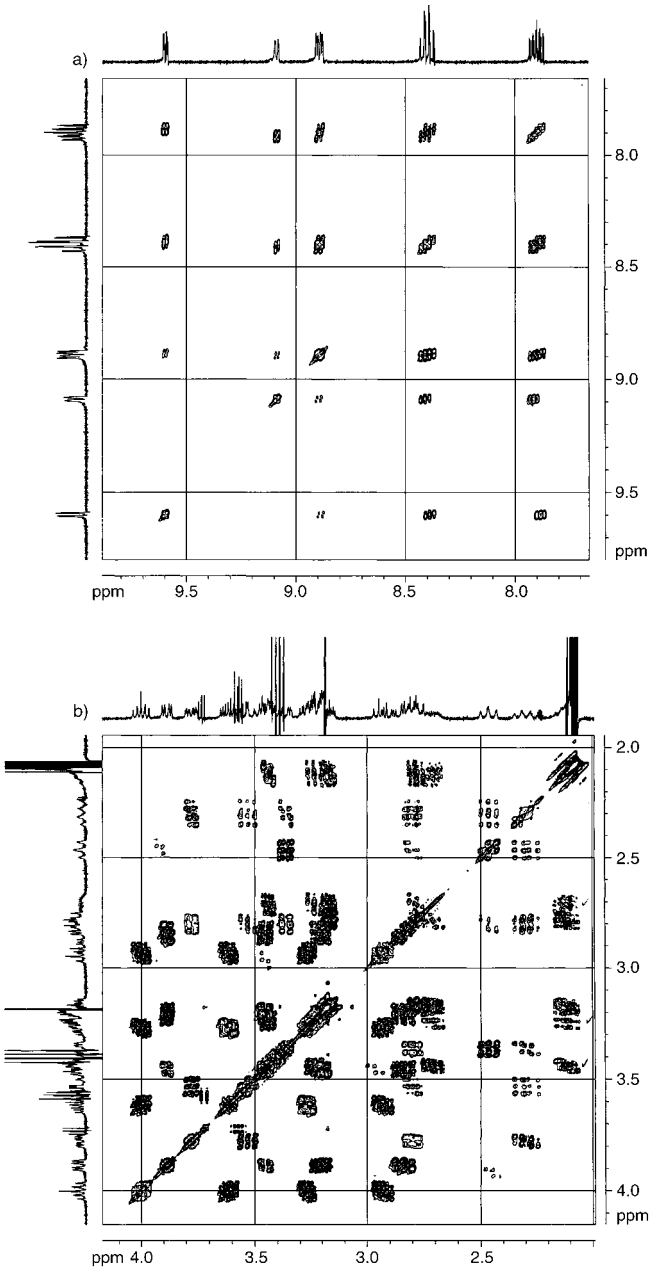

Figure 8. The 400 MHz COSY-45 ^{1}H NMR spectrum of **4**-$(PF_6)_2$ in [D_6]acetone at −15 °C: a) aromatic signals; b) thiacrown signals.

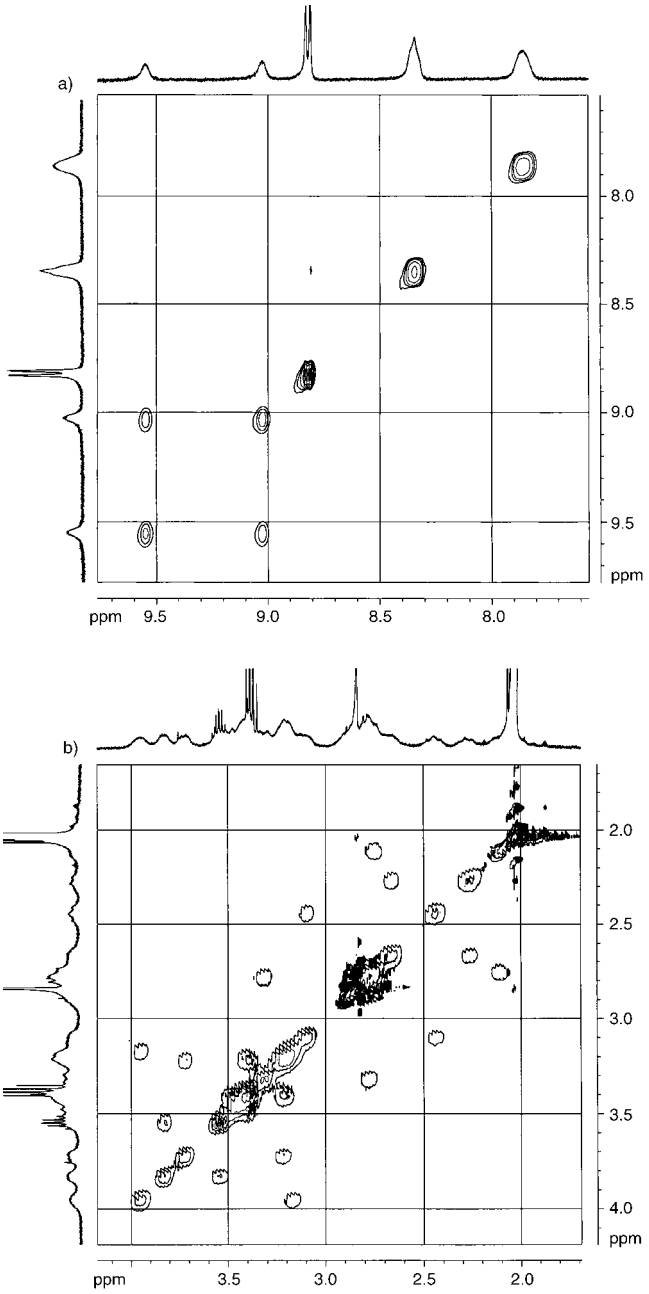

Figure 9. The 400 MHz EXSY ^{1}H NMR spectrum of **4**-$(PF_6)_2$ in [D_6]acetone at room temperature (20 °C) with a mixing time of 0.03 s and a relaxation delay of 5 s: a) aromatic signals; b) thiacrown signals.

served exchange is consistent with the inversion of both sulfur atoms in **4b**, resulting in pairwise exchange of the two types of six-membered rings and similarly, the two types of five-membered rings. Quantitative analysis of the EXSY spectrum yielded rates of 20 s^{-1} corresponding to a $\Delta G^{\ddagger}_{293}$ of 64 ± 2 kJ mol^{-1}. The increased $\Delta G^{\ddagger}$ compared with that observed for **1** is attributed to a mechanism involving **4a** or **4c**. Neither of these isomers are observed in solution, so they must lie at least 4 kJ mol^{-1} above **4b**, resulting in the increased $\Delta G^{\ddagger}$ relative to **1**.

At room temperature the ^{1}H spectrum of **5**-$(PF_6)_2$ in [D_6]acetone shows one set of signals. On cooling, the ^{1}H NMR spectrum initially broadens and then at −90 °C shows signals attributable to two isomers. The room temperature and −90 °C ^{1}H NMR spectra are shown in Figure 10. The resolution is best for H^6, which clearly shows signals due a major isomer with two inequivalent H^6 protons at $\delta =$ 9.85 and 9.45 ppm and a minor isomer at $\delta = 9.27$ ppm in the ratio 1:0.35, corresponding to $\Delta G^{\ddagger}_{183} = 1.6$ kJ mol^{-1}. The resolution is poor for the remaining protons.

A COSY spectrum was also measured at −90 °C, see Figure 11. This provided further information on the assignment of the signals, especially those of the bpy ligand, but

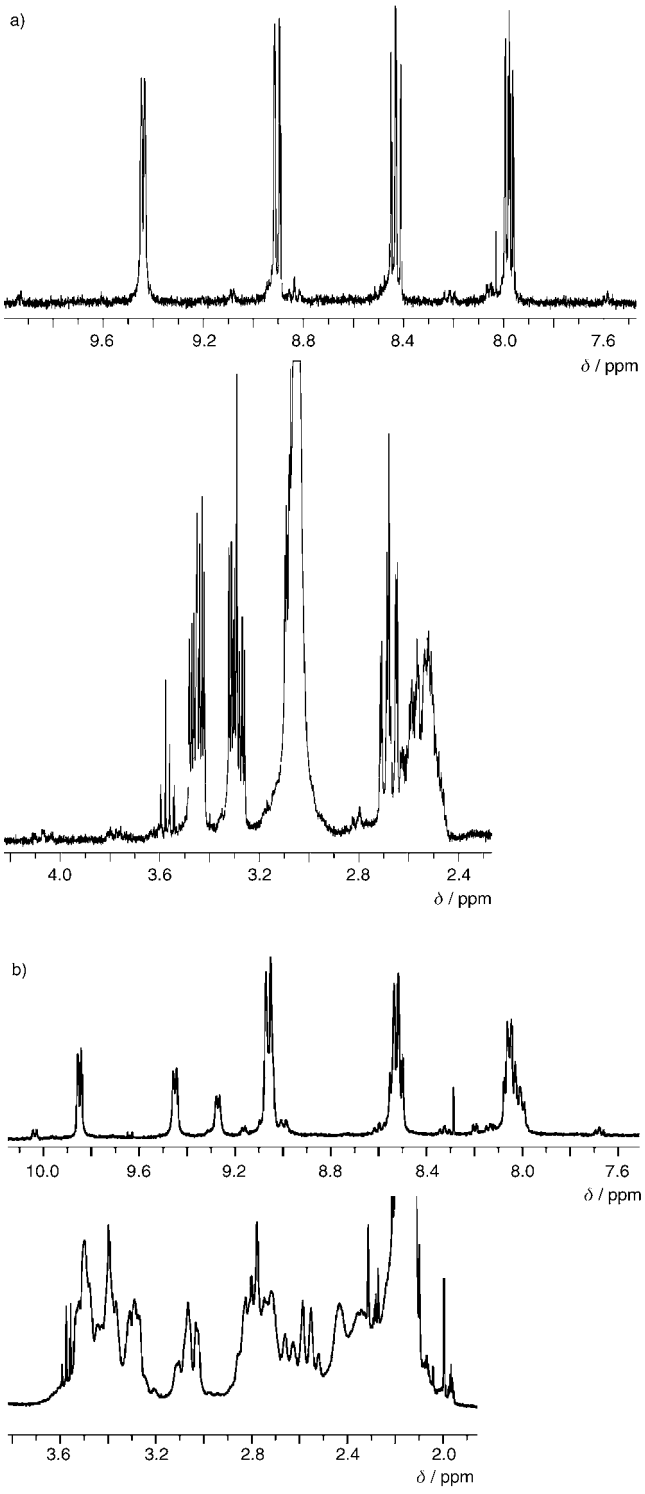

Figure 10. The 400 MHz ^{1}H NMR spectrum of **5**-$(PF_6)_2$ in [D_6]acetone: a) at room temperature; b) at −90 °C.

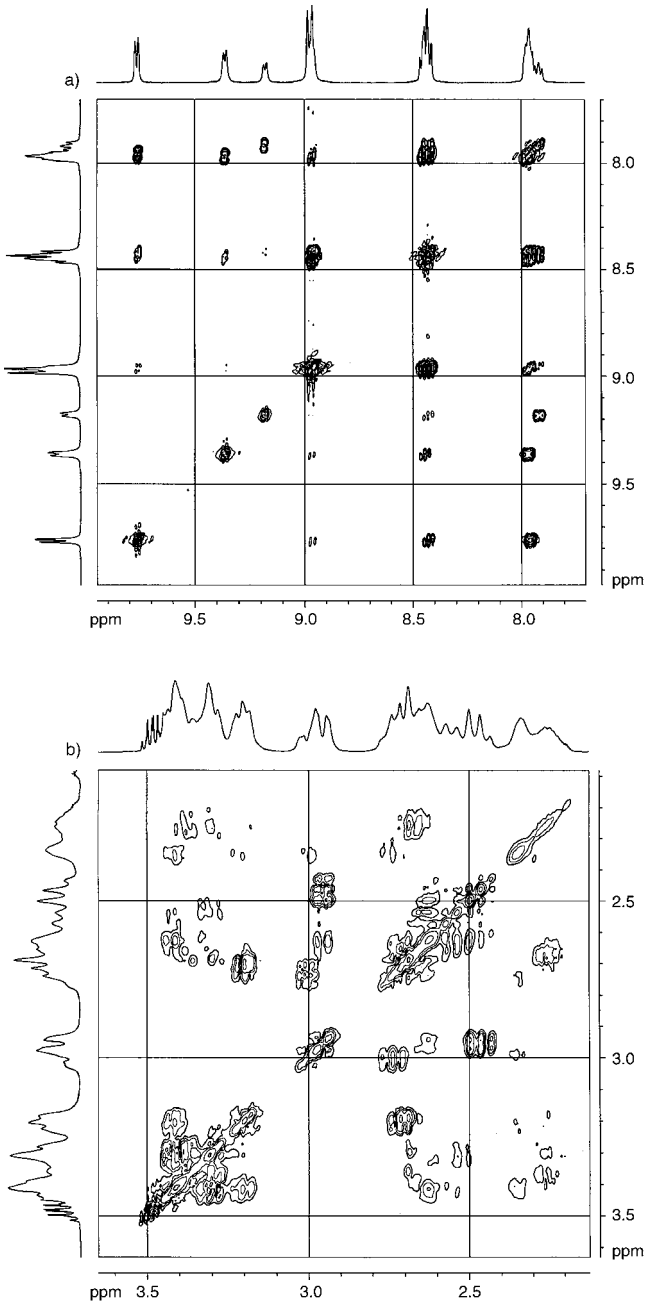

Figure 11. The 400 MHz COSY-45 ^{1}H NMR spectrum of **5**-$(PF_6)_2$ in [D_6]acetone at −74 °C: a) aromatic signals; b) thiacrown signals.

failed to give sufficient information to determine the conformation of L[3].

Quantitative exchange information was obtained from a ^{1}H EXSY spectrum at −74 °C. The relaxation delay of 2.5 s is $5T_1$ and the mixing delay of 0.03 s is short compared with relaxation to minimize NOE contributions. The resulting spectrum is given in Figure 12. Weak signals are present, but as the EXSY spectrum fails to show any cross peaks with the major isomers, it is believed that they arise from the unidentified compounds/isomers observed at room temperature.

A quantitative analysis of the ^{1}H EXSY spectrum in Figure 12 yielded $10.1 \pm 1.5\ s^{-1}$ as the rate of major to minor isomer excahnge and $29 \pm 2.0\ s^{-1}$ as the rate of minor to major isomer exchange. This corresponds to $\Delta G^{\ddagger}_{199} = 44.3 \pm$

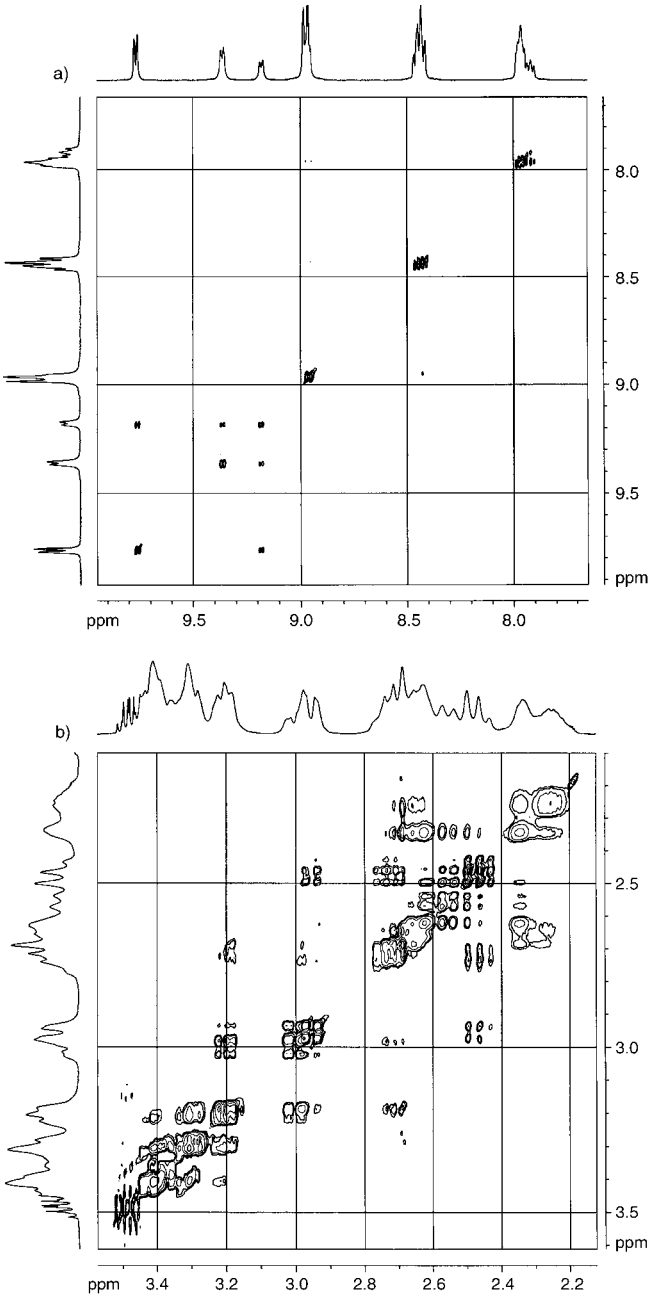

Figure 12. The 400 MHz EXSY ^{1}H NMR spectrum of **5**-$(PF_6)_2$ in $[D_6]$acetone at −74 °C with a mixing time of 0.03 s and a relaxation delay of 2.5 s: a) aromatic signals; b) thiacrown signals.

0.5 kJ mol^{-1} for the major isomer removal and 42.5 ± 0.5 kJ mol^{-1} for the minor isomer removal.

These $\Delta G^{\neq}$ values are much lower than those observed for **1**, **4**, and **6**. This raises the possibility that the fluxionality could be due to either sulphur inversion or exchange between boat and chair conformations of the $[CH_2(CH_2S_2)_2Ru]$ rings. For example, ring inversion occurs with $\Delta G^{\neq}_{199}$ = 31 kJ mol^{-1} for **7**.[27]

The crystal structure of **5**-$(PF_6)_2$ shows some disorder (Figure 2), but the structure of the cation is clearly **5b**. In **5b** the two pyridyl groups are inequivalent, which is consistent with the major isomer in the NMR spectrum. In the minor isomer, the two pyridyl rings are equivalent. The ^{1}H NMR spectra of the [16]ane-S_4 ligand are too complex to assign the signals, preventing further information being obtained about the structures of the two isomers by using this technique.

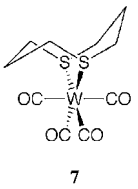

7

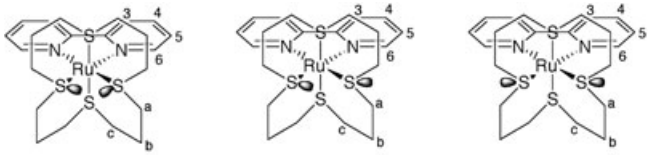

5a 5b 5c

Complex **5a** has the coordination geometry normally adopted by L^3, for example, it is observed in $[NiCl(L^3)]_2(BF_4)_2$.[17] The geometry found in **5c** has not been observed crystallographically.

The value of $\Delta G^{\neq}_{199}$ observed for the dynamic process in **5**-$(PF_6)_2$ could either arise from sulfur or six-membered ring inversion. The problem could not be resolved by NMR spectroscopy on account of the complexity of the spectra. In order to shed light on this question, modeling studies were performed.

Modeling studies: While the degree of geometrical distortion of the new complexes from the ideal octahedron appears to reflect the different cavity sizes of these three crown thioethers, the conformational preferences exhibited by the macrocycles in solution and solid phase are puzzling. Previously, density functional theory (DFT) calculations have provided relevant information concerning the structure and energetics of macrocyclic and thio complexes.[28] In order to rationalize the conformational preferences of the [*n*]ane-S_4 macrocycles in the $[Ru([n]ane\text{-}S_4)(bpy)]^{2+}$ complexes, DFT calculations were performed by using the program Gaussian 98.[15]

The crystal structure of **1**-Cl_2 reveals that the macrocycle displays a well-defined **c** conformation thus allowing the comparison with the calculated **1c** structure. To investigate the validity of computational studies we started DFT calculations with a full optimization of the X-ray structure of **1**. A comparison of the selected bond distances and angles derived from experimental and computational data, presented in Figure 13, shows a close similarity between both structures.

Furthermore, fitting between the atomic coordinates of experimental and calculated structure, excluding hydrogen atoms, gives a root-mean-square (RMS) value of 0.0578 Å,

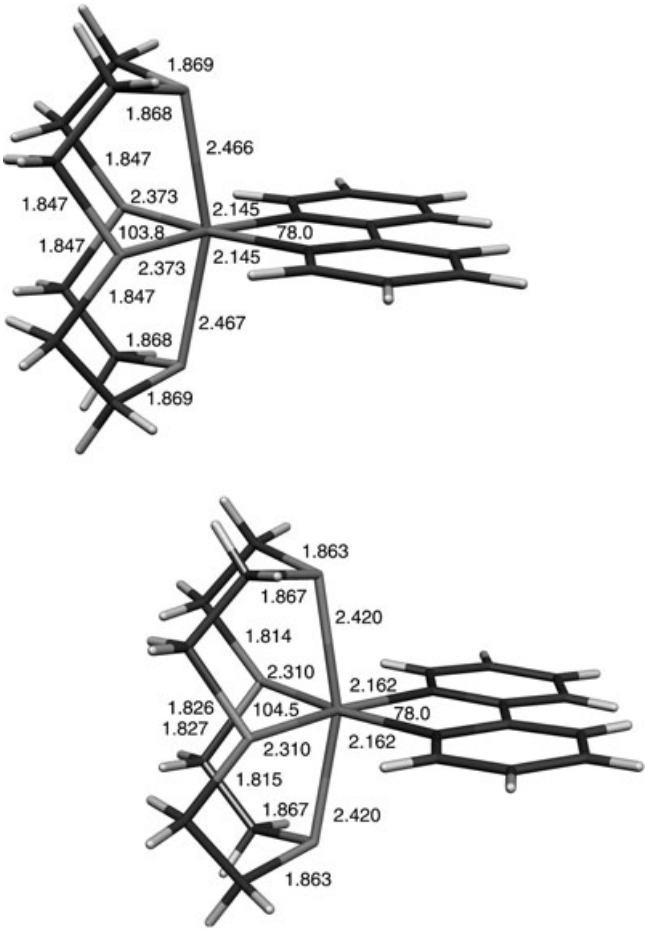

Figure 13. Comparison of the X-ray (bottom) and DFT (top left) structures of the complex **1** in the isomeric form **1c**. The axial S-Ru-S angle is 162.5° and 160.6° for X-ray and DFT structures, respectively.

Table 6. Selected distances [Å] and angles [°] for DFT-computed minimum energy invertomers of the $\mathbf{1}^{2+}$ cation.

	a	**b**	**c**
bond lengths			
Ru–S_{ax}	2.428, 2.428	2.449, 2.451	2.466
Ru–S_{eq}	2.378, 2.378	2.371, 2.381	2.373
Ru–N	2.155, 2.155	2.146, 2.130	2.145, 2.145
C–S	1.856–1.897	1.852–1.890	1.847–1.869
bond angles			
N–Ru–N	77.1	77.7	78.0
S_{ax}–Ru–S_{ax}	166.7	163.8	160.5
S_{eq}–Ru–S_{eq}	81.4	88.4	103.8
S_{eq}–Ru–N	100.7, 100.7	102.2, 91.6	89.1, 89.1
intramolecular distances			
S_{eq}···H	2×2.948	2.544, 2.940	2.502, 2.497
S_{eq}···S_{eq}	3.106	3.426	3.764

Table 7. Selected distances [Å] and angles [°] for DFT-computed minimum energy invertomers of the $\mathbf{4}^{2+}$ cation.

	a	**b**	**c**
bond lengths			
Ru–S_{ax}	2.419, 2.420	2.430, 2.434	2.424, 2.424
Ru–S_{eq}	2.411, 2.411	2.397, 2.405	2.396, 2.396
Ru–N	2.133, 2.133	2.125, 2.132	2.135, 2.135
C–S	1.847–1.856	1.843–1.874	1.844–1.858
bond angles			
N–Ru–N	77.6	77.9	78.0
S_{ax}–Ru–S_{ax}	176.8	175.5	174.0
S_{eq}–Ru–S_{eq}	80.2	89.1	100.6
S_{eq}–Ru–N	101.2,101.0	91.9, 101.4	90.7, 90.7
intramolecular distances			
S_{eq}···H	2.932, 2.934	2.954, 2.546	2.521, 2.521
S_{eq}···S_{eq}	3.107	3.368	3.687

Table 8. Selected distances [Å] and angles [°] for DFT-computed minimum energy invertomers of the $\mathbf{5}^{2+}$ cation.

	a	**b**	**c**
bond lengths			
Ru–S_{ax}	2.440, 2.440	2.444, 2.442	2.451, 2.429
Ru–S_{eq}	2.453, 2.453	2.432, 2.433	2.420, 2.415
Ru–N	2.113, 2.113	2.129, 2.124	2.139, 2.144
C–S	1.846–1.861	1.844–1.862	1.842–1.862
bond angles			
N–Ru–N	78.3	78.0	77.8
S_{ax}–Ru–S_{ax}	171.7	174.1	176.6
S_{eq}–Ru–S_{eq}	78.6	89.5	102.3
S_{eq}–Ru–N	101.8, 101.8	91.6, 101.1	90.0, 90.0
intramolecular distances			
S_{eq}···H	2×2.948	2.544, 2.940	2.502, 2.497
S_{eq}···S_{eq}	3.106	3.426	3.764

indicating that all structural features of the X-ray determination are reproduced in the computational model. For example, the bond distances have a pattern consistent with the C_2 symmetry observed crystallographicaly, even though this symmetry constraint had not been imposed in the DFT optimization.

As these results indicate that the basis used is appropriate to model the stereoelectronic properties of [Ru([*n*]ane-S_4)(bpy)]$^{2+}$ complexes, calculations were extended to model conformations consistent with the isomeric forms **1b** or **1c**, and also the postulated invertomers of **4** and **5**. The optimized structures of the **a**, **b**, and **c** isomers, together with their relative energies, are shown in Figure 14. The group symmetry of each structure is also given in the figure.

Calculated distances and angles in the metal coordination of these complexes, as well as the C–S distances for the three isomeric forms are compared in Tables 6, 7, and 8.

The calculations on the three cations place the three isomeric forms in a stability order that is agreement with X-ray data available from structural data for M([*n*]ane-S_4) complexes (M = metal ion). The latter data reveals that complexes of the macrocycles adopt a folding conformation, encapsulating the transition metal in a *cis*-octahedral environment. The macrocycles L^2 and L^3 adopt **a** or **b** conformations, while the macrocyle L^1 prefers **b** or **c** conformations. In addition, the relative energies computed for these folded conformations are in reasonable agreement with the experimental energy values derived from the solution phase NMR data (keeping in mind that DFT calculations refer to isolat-

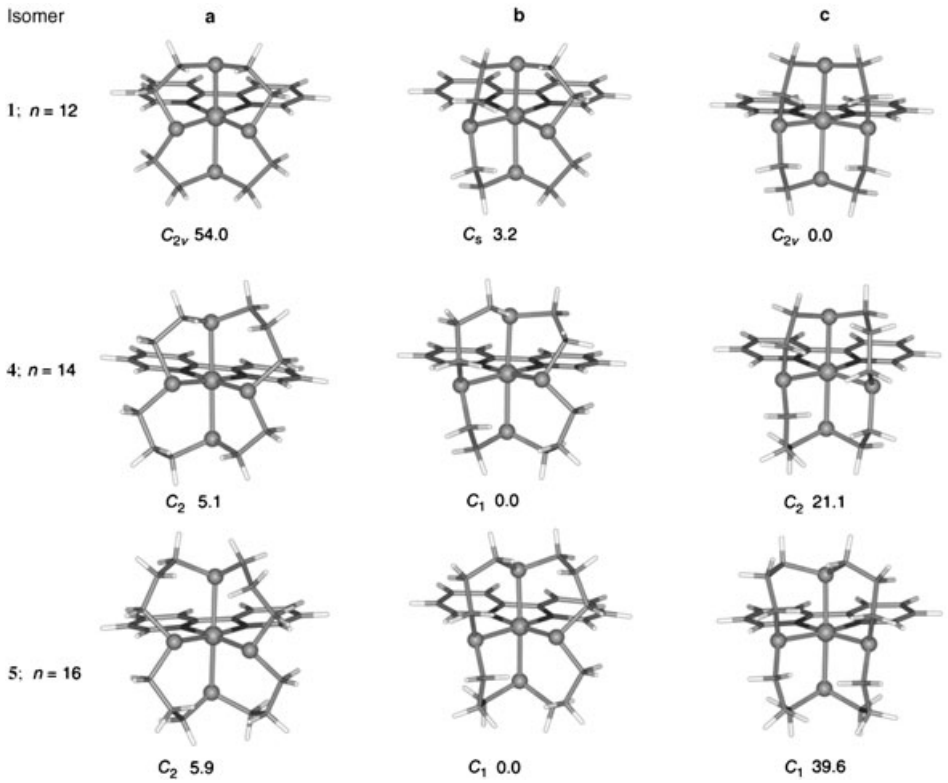

Figure 14. DFT-computed minimum energy structures of the three isomers **a**, **b**, and **c** for complexes $[Ru([n]ane\text{-}S_4)(bpy)]^{2+}$ with their relative energies ($kJ\,mol^{-1}$).

ed molecules, the condensed phase effects, such as solvent or crystal packing effects, were therefore not taken into account).

The DFT calculations on **1** yielded isomer **1c**, observed experimentally as the most stable form, but only by 3.2 $kJ\,mol^{-1}$ relative to **1b**. The optimized structure of **1a** corresponds to a local minimum 54.9 $kJ\,mol^{-1}$ higher in energy. These results are consistent with the NMR data, which reveal the presence of two forms in solution, assigned to **1c** and **1b**, with a ΔG°_{230} separation of 3.5 $kJ\,mol^{-1}$ (the comparison between ΔE and ΔG values assumes similar thermal energy corrections, including zero-point vibrational energy, for the three conformations).

In contrast to **1**, calculations indicate that for **4** and **5**, the stability of isomeric forms follows the order **b** > **a** > **c**. Thus, for complex **4**, the isomer **4b** is favored relative to isomers **4a** and **4c** by 5.1 and 21.1 $kJ\,mol^{-1}$, respectively. While the **c** conformation of L^2 does not appear to have been observed crystallographically, NMR results suggest that **4b** is the only species present in the solution of **4**. For complex **5**, the most stable form, **5b**, is below forms **5a** and **5c** by 5.9 and 39.6 $kJ\,mol^{-1}$, respectively. While the former value of 5.9 $kJ\,mol^{-1}$ is above the experimentally derived ΔG°_{183} value, the NMR spectrum of **5** shows the presence of two isomers, which, in view of the DFT results, may be assigned to the **5b** and **5a** invertomers.

Other structural features revealed by the DFT calculations deserve some discussion. In L^1 metal transition complexes with *cis*-octahedral geometry, the small cavity size of the folded macrocycle prevents two sulfur donor atoms from achieving idealized positions. This leads to $Ru{-}S_{ax}$ distances being longer than equatorial distances and S_{ax}-Ru-S_{ax} angles that are considerably smaller than 180°.[29] Both structural features are clearly apparent from the optimized geometries of **1a**, **1b**, and **1c**.

As the size of the macrocycle increases from 12- to 16-membered rings, the difference between the $Ru{-}S_{ax}$ and $Ru{-}S_{eq}$ distances becomes much less pronounced and the S_{ax}-Ru-S_{ax} angle should approach that of a perfect octahedron. This trend is observed in all the calculated structures for the three isomeric forms of **1**, **4**, and **5**. In fact, when geometric parameters are compared, only slight differences are observed between isomers of the latter two complexes. Therefore, it is almost impossible to decide from DFT data which of the macrocycles (L^2 or L^3) has the cavity with the most appropriate size to accommodate an Ru center in a *cis*-octahedral environment. All computed structures display similar Ru–N distances and the corresponding N-Ru-N angles differ less than 1.3°, which is a consequence of the stereoelectronic demands of the small bite angle of bpy. It is clear that the values of the remaining *cis* angles of the equatorial plane S_{eq}-Ru-S_{eq} and S_{eq}-Ru-N_{eq} depend on the orientation of the electron lone pairs of the two equatorial sulfur donor atoms rather than the macrocyclic dimensions. For example, **1a** has two lone pairs in an *endo* configuration and the S_{eq}-Ru-S_{eq} angle is 81.4°, while in isomer **1c** the two electron pairs are *exo* and the angle is forced to become more open, taking a value of 103.8°. Isomer **1b** with one electron lone pair in an *endo* position and one in an *exo* position has an intermediate angle of 88.0°. As expected, the reverse situation is observed for both S_{eq}-Ru-N_{eq} angles. Thus, for isomer **1b**, the angle involving the *endo* sulfur atom is similar to those found for isomer **1a**, while the angle involving the *exo* sulfur atom is identical to those found for isomer **1c**. The same structural trend, with similar values, is followed by geometric isomers of **4** and **5**. These observations indicate that the degree of the folding of the macrocycle along the axis defined by the two axial sulfur donor atoms is more pronounced in type **a** isomers and reflects the conformation adopted by the macrocycle rather than the cavity size of the ligand. In line with these observations, the $S_{eq}\cdots S_{eq}$ and

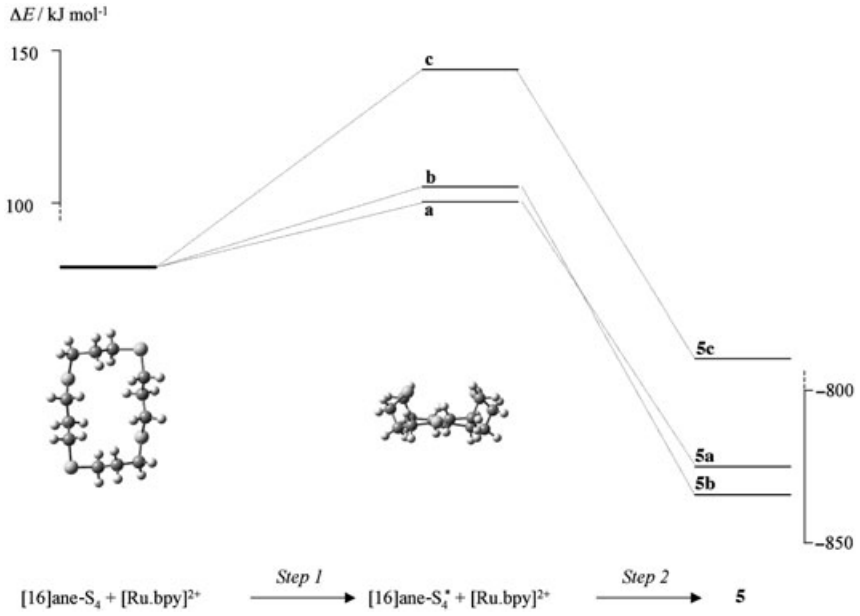

Figure 15. Two-step mechanism illustrating the formation of the geometric isomers for complex **5**.

S_{eq}···H (in which H represents the H^6 and $H^{6'}$ atoms on the bpy ring) intramolecular distances observed are also dependent on macrocyclic conformation (see Tables 6–8).

To fully understand this stability order, it is useful conceptually to assume that the formation of **1**, **4**, and **5** occurs through a two-step mechanism: in the first step, the free macrocycle adopts a folded conformation consistent with the **a**, **b**, or **c** configuration (a structural "pre-organization" step); subsequently in the second step, the macrocycle, in the "pre-organized" conformation, binds the Ru–bpy fragment (macrocycle "complexation" step) to give one of the geometric isomers. This mechanism is illustrated for the three geometric isomers of complex **5** in Figure 15. In this process, the "pre-organization" energy is given by Equation (1):

$$\Delta E = E_1 - E_2 \quad (1)$$

in which E_1 represents the energy of the macrocycle in the complex (single point energy) and E_2 is the energy of the optimized structure of free macrocycles. Both terms also include the energy of the separated Ru–bpy fragment allowing the comparison with the energies of entire complexes. In all cases except one, the observed conformational preferences are determined by the energy required to pre-organize the conformation of the macrocyclic ligand in order to fit the stereoelectronic demands of the metal center. The energy involved in the "complexation" step is nearly identical for all isomers and so the energy order between them is retained. The exception to this behavior is observed for the **5a**/**5b** pair. In the "pre-organization" step, form **a** is more stable than form **b** by 3.1 kJ mol^{-1}, but after the "complexation" step the order is reversed by 5.9 kJ mol^{-1}. All these effects can be explained in terms of intramacrocycle and macrocycle–bpy steric interactions involving short H···H contacts, with only localized contributions from electronic distribution.

Figure 16 presents DFT-computed minimum energy molecular diagrams for [Ru([*n*]ane-S_4)(bpy)]$^{2+}$ fragments showing the close contacts between hydrogen atoms separated by at least three non-hydrogen atoms and using a cut-off value of 2.4 Å (sum of van der Waals radii of two hydrogen atoms). In conformation **1a**, all -CH_2-$S_{ax}CH_2$- and -$CH_2S_{eq}CH_2$- groups adopt eclipsed arrangements leading to C_{2v} symmetry for this isomer with two symmetry planes running along and perpendicular to the bpy ligand. The *endo* orientation of the two equatorial sulfur lone pairs brings -CH_2S_{eq} into four close contacts of 1.94 Å with the H−(C−N) atoms from bpy. In addition, a second close contact of 2.11 Å occurs between the two hydrogen atoms of each -$CH_2S_{ax}CH_2$- fragment. By contrast, for isomer **1c**, in which electron lone pairs of both equatorial sulfur atoms adopt an *exo* configuration, only the latter type of interactions are observed, with short intramolecular distances of 2.03 Å. These interactions involve two -CH_2S_{eq} groups from consecutive five-membered chelate rings.

Isomer **1b** displays nearly C_s symmetry with the symmetry plane containing the bpy ligand. As expected, only the CH_2 groups from the -$CH_2S_{eq}CH_2$- fragment with the sulfur atoms in a *endo* configuration are involved in close contacts with bpy through one of the -N−C−H groups, resulting in two intramolecular distances of 1.95 and 1.96 Å. In this structure, two CH_2 groups from each -$CH_2S_{ax}CH_2$- fragment exhibit an almost staggered conformation, with two short contacts of 2.37 Å between them. These results suggest that the relative stability of the three isomeric forms of [Ru([12]ane-S_4)(bpy)]$^{2+}$ are related to the number and strength of the intramolecular contacts described. Thus, for the **c**, **b**, and **a** isomeric forms, with two, four, and six intramolecular contacts, respectively, the steric stability decreases in the following order **c** > **b** > **a**.

As already found for **1c**, isomers **4c** and **5c** show no close contacts between bpy hydrogens and those of the macrocyclic framework. However, as the macrocycle becomes larger, the number of unfavorable interactions between hydrogen atoms within the macrocyclic framework increases to five for **4c** and six for **5c**. In both cases, this isomer now becomes the higher energy form, thus altering the stability order to **b** > **a** > **c**.

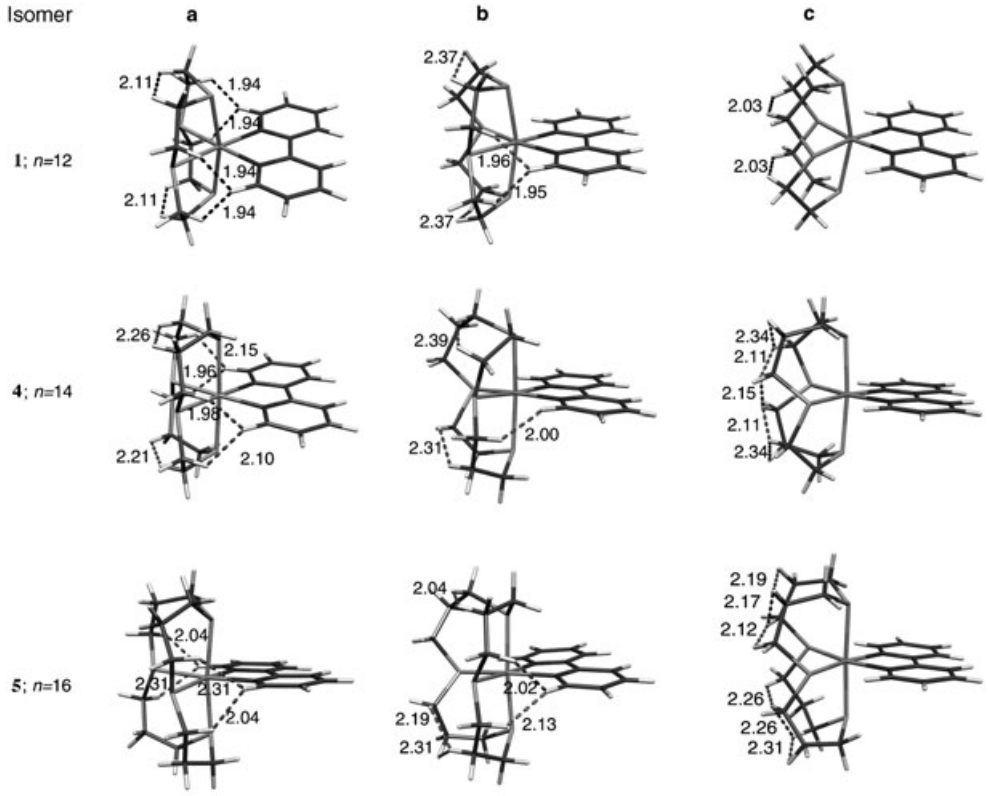

Figure 16. DFT structures of the three isomers **a**, **b**, and **c** for complexes $[Ru([n]ane\text{-}S_4)(bpy)]^{2+}$ ($n=12$, 14, or 16) showing the H···H intramolecular close contacts.

In order to further study the invertomers of **1**, **4**, and **5**, the frontier orbitals of the relevant isomers were investigated. With the exception of **5b**, all calculated structures display very similar frontier orbitals. Figure 17 (from left to right) shows the HOMO and HOMO−1 orbitals for isomer **5a** and the HOMO orbital for isomer **5b**. The HOMO of **5a** is concentrated on the d_{xz} orbital of the metal center and two orbitals from the axial sulfur donor atoms, which are the result of the combination of the p_x and p_z orbitals. The HOMO−1 of **5a** comprises the orbital $d_{x^2-y^2}$ from Ru^{II} and two molecular orbitals derived from the interaction between the p_y and s atomic orbitals from equatorial sulphur donor atoms. The HOMO for **5b** is obtained in a different way: the d_{xz}, d_{z^2}, and $d_{x^2-y^2}$ orbitals from the metals interact with the orbitals p_x and p_z from axial sulphur atoms. Given the small differences in frontier orbitals, these results suggest that the conformational preferences of the three macrocyles in $[Ru([n]ane\text{-}S_4)(bpy)]^{2+}$ complexes are essentially determined by steric rather than electronic effects.

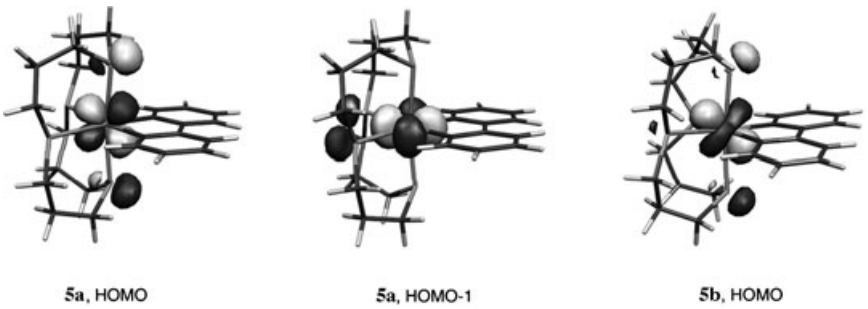

Figure 17. Molecular orbitals for $[\mathbf{5}]^{2+}$.

Another interesting point that can be addressed by DFT calculations concerns the "interconversion" process between isomers and $\Delta G^{\neq}$ values obtained experimentally from NMR studies. Ab initio calculations for the first-order saddle points (transition states) between the two most stable isomers have been carried out. The transition states correspond to the inversion of the sulfur moiety through a planar structure. The planarity around the S atom in the transition state can be evaluated by the sum of the valence angles Ru-S-C and C-S-C, which

in all cases match $360 \pm 0.1°$ (C-S-C angles are 124.0° in **1**, 116.8° in **3**, and 108.1° in **4**, while Ru-S-C angles range from 113.0° to 130.2°). The corresponding molecular orbitals clearly confirm the trigonal geometry around the S atom.

The calculated interconversion energy barrier, $\Delta E^{\neq}$, between the two lowest energy forms does not show a linear dependence on the size of the three macrocycles considered. This is not surprising as transition states are not between the same isomers.

In general, taking into account the different meanings of the energy functions and the exclusion of solvent effects, ab initio interconversion energy barriers are in good agreement with the corresponding experimentally derived $\Delta G^{\neq}$ values. For compound **1**, the barrier between **1b** and **1c** was found to be approximately 68 kJ mol^{-1}, which is comparable to $\Delta G^{\neq}_{230} = 56 \pm 2$ kJ mol^{-1}. For complex **4**, the calculated value of approximately 76 kJ mol^{-1} has no experimental counterpart and can only be compared to the $\Delta G^{\neq}_{293}$ value of 64 ± 2 kJ mol^{-1} reported for the inversion of both sulfur atoms in isomer **4b**. The lowest energy barrier value is found for complex **5**, a feature that can be related to the additional flexibility resulting from the larger macrocycle. Calculated $\Delta E^{\neq}$ and experimental $\Delta G^{\neq}_{199}$ values are 54 kJ mol^{-1} and 44.3 ± 0.5 kJ mol^{-1}, respectively.

Conclusion

Although free L^1, L^2, and L^3 have considerable conformational flexibility, the calculated structures reveal that the steric constraints of assembling each of the macrocycles, as well as a bpy ligand, around the octahedral Ru^{II} coordination sphere, lead to close intramolecular H···H contacts in all isomeric forms. These contacts are largely dependent on the orientation of the electron lone pairs of equatorial sulfur donor atoms and correlate with the comparative stability of the different invertomeric forms of complexes **1**, **4**, and **5**. Future synthetic work will concentrate on the synthesis of oligomeric structures incorporating [Ru([*n*]ane-S_4)] fragments, while DFT calculations will center on a more detailed study on the electronic structure of such complexes. Structural studies to investigate how generally applicable these observations are to other macrocyclic coordination complexes are also underway.

Experimental Section

Materials: The complexes *cis*-[Ru(dmso)$_4$Cl$_2$],[11] [Ru(dmso)Cl(L^1)]PF_6,[9] and **1**-$(PF_6)_2$[9] were prepared according to previously published procedures. All other reagents were obtained commercially and used as supplied. Reactions were conducted under an atmosphere of nitrogen. Products were dried at room temperature in a vacuum desiccator for approximately 10 h prior to characterization.

Physical measurements: ^{1}H NMR spectra were recorded on a Bruker AM250 or AMX400 NMR spectrometer. Spectra were acquired in a range of 0–12 ppm with 32 K data points. The temperature was determined using a Comark electronic thermometer with a thermocouple in an NMR tube containing the same solvent as the NMR sample. ^{1}H EXSY spectra were obtained using the phase-sensitive Bruker pulse sequence noesytp. Quantitative analyses of the resultant ^{1}H EXSY spectra were carried out using a computer program supplied by Dr. K. Orrell.[12] FAB mass spectra were obtained on a Kratos MS80 machine working in positive-ion mode, with a *m*-nitrobenzyl alcohol matrix. Elemental analyses were obtained using a Perkin–Elmer 2400 analyzer working at 975 °C.

Syntheses

[Ru(dmso)Cl(L^2)]PF_6, 2-PF_6: A mixture of *cis*-[Ru(dmso)$_4$Cl$_2$] (0.485 g, 0.1 mmol) and L^2 (0.268 g, 1 mmol) were dissolved in ethanol/water (1:1, 20 mL). The solution was brought to reflux for 4 h. After cooling to room temperature, excess solid NH_4PF_6 was added to the reaction mixture. This solution was left overnight at 2 °C. The resultant precipitate was washed with water and then ethanol. It was then dried in vacuo to yield **2**-PF_6 as a pale-yellow microcrystalline powder (0.471 g, 75 %). ^{1}H NMR ([D$_6$]acetone): $\delta = 3.5$–2.35 ppm (m, 20H); FAB MS: *m*/*z* (%): 483 (25) [$M^+ - PF_6$], 405 (43) [$M^+ - PF_6 - DMSO$]; elemental analysis calcd (%) for $RuC_{12}H_{26}S_5ClOPF_6$: C 22.94, H 4.17, S 25.52; found: C 23.31, H 4.27, S 24.93.

[Ru(dmso)Cl(L^3)]PF_6, 3-PF_6: A mixture of *cis*-[Ru(dmso)$_4$Cl$_2$] (0.485 g, 0.1 mmol) and L^3 (0.297 g, 1 mmol) were dissolved in ethanol/water (1:1, 20 mL). The solution was brought to reflux for 4 h. After cooling to room temperature, excess solid NH_4PF_6 was added to the reaction mixture. This solution was left overnight at 2 °C. The resultant precipitate was washed with water and then ethanol. It was then dried in vacuo to yield **3**-PF_6 as a pale-yellow microcrystalline powder (0.446 g, 68 %). ^{1}H NMR ([D$_6$]acetone): $\delta = 3.35$–2.2 ppm (m, 24H); FAB MS: *m*/*z* (%): 511 (32) [$M^+ - PF_6$]; elemental analysis calcd (%) for $RuC_{14}H_{30}S_5ClOPF_6$: C 25.62, H 4.61, S 24.43; found: C 26.02, H 4.72, S 24.68.

[Ru(L^2)(bpy)]$(PF_6)_2$, 4-$(PF_6)_2$: A solution of **2**-PF_6 (0.3 g, 0.4775 mmol) in ethanol/water (1:1, 20 ml) was brought to reflux. $AgNO_3$ (0.105 g, 1.3 equiv) was added to the yellow solution and the mixture was left at reflux for 4 h. After removal of AgCl by filtration, excess 2,2′-bipyridine (0.149 g, 2 equiv) was added to the mixture and was then brought to reflux for a further 3 h. After cooling to room temperature, excess solid NH_4PF_6 was added to the reaction mixture. The volume of the solution was reduced in vacuo to 10 ml and then left overnight at 2 °C. The resultant precipitate was washed with ethanol, diethyl ether, and then dried in vacuo to yield **4**-$(PF_6)_2$ (0.316 g, 81 %). ^{1}H NMR (RT, [D$_6$]acetone): bpy protons: $\delta = 9.60$ (ddd, $J_{5,6} = 5.8$, $J_{4,6} = 1.5$, $J_{3,6} = 0.7$ Hz; H^6), 9.09 (dd, $J_{5',6'} = 5.7$, $J_{4',6'} = 1.4$ Hz; $H^{6'}$), 8.89 (ddd, $J_{3,4} = 8.5$, $J_{3,5} = 1.4$, $J_{3,6} = 0.7$ Hz; H^3), 8.89 (dd, $J_{3',4'} = 8.4$, $J_{3',5'} = 1.5$ Hz; $H^{3'}$), 8.41 (dt, $J_{3',4'} = J_{4',5'} = 8.2$, $J_{4',6'} = 1.5$ Hz; $H^{4'}$), 8.39 (dt, $J_{3,4} = J_{4,5} = 8.2$, $J_{4,6} = 1.5$ Hz; H^4), 7.91 (ddd, $J_{4',5'} = 7.7$, $J_{5',6'} = 5.7$, $J_{3',5'} = 1.4$ Hz; $H^{5'}$), 7.89 ppm (ddd, $J_{4,5} = 7.6$ Hz, $J_{5,6} = 5.8$ Hz, $J_{3,5} = 1.4$ Hz; H^5); 14-ane-S_4 protons: $\delta = 4.00$ (ddd, $^2J = 13.5$, $^3J = 6.5$, 8.0 Hz; $CH_2^{d,e}$), 3.88 (dd, $^2J = 11.5$, $^3J = 4.0$, < 1 Hz; $CH_2^{d',e'}$), 3.78 (ddd, $^2J = 12.5$, $^3J = 2.0$, 5.5 Hz; $CH_2^{a,c}$), 3.62 (ddd, $^2J = 13.5$, $^3J = 4.0$, 8.5; $CH_2^{d,e}$), 3.53 (dt, $^2J = 12.5$, $^3J = 2.0$, 12.5 Hz; $CH_2^{a,c}$), 3.46 (obscured; $CH_2^{e',d'}$), 3.45 (obscured; $CH_2^{a',c'}$), 3.36 (ddd, $^2J = 14$, $^3J = 4$, ca. 1 Hz; $CH_2^{a,c}$), 3.27 (ddd, $^2J = 14.5$, $^3J = 4.5$, 6.5 Hz; $CH_2^{e,d}$), 3.25 (obscured; $CH_2^{a',c'}$), 3.20 (obscured; $CH_2^{d',e'}$), 3.18 (obscured; $CH_2^{e',a'}$), 2.93 (dt, $^2J = 14.5$, $^3J = 7$, 7 Hz; $CH_2^{e,d}$), 2.84 (dt, $^2J = 15.0$, $^3J = 15.0$, 4.5 Hz; $CH_2^{e',d'}$), 2.80 (obscured; CH_2^{b}), 2.78 (obscured; $CH_2^{a',c'}$), 2.70 (obscured; CH_2^{b}), 2.47 (t, $^2J = 14$, $^3J = 14$, < 2 Hz; $CH_2^{a,c}$), 2.30 (ttq, $^2J = 13$, $^3J =$ ca. 1.5, ca. 1.5, 13, 13 Hz; CH_2^{b}), 2.12 ppm (obscured; $CH_2^{b'}$); FAB MS: *m*/*z* (%): 671 (100) [$M^+ - PF_6$]; elemental analysis calcd (%) for $RuC_{20}H_{30}N_2S_4OP_2F_{12}$ (**4**-H_2O): C 28.81, H 3.63, N 3.36, S 15.38; found: C 28.37, H 3.87, N 3.65, S 14.97.

[Ru(L^3)(bpy)]$(PF_6)_2$, 5-$(PF_6)_2$: A solution of **3**-PF_6 (0.3 g, 0.4571 mmol) in ethanol/water (1:1, 20 ml) was brought to reflux. $AgNO_3$ (0.101 g, 1.3 equiv) was added to the yellow solution and the mixture was left at reflux for 4 h. After removal of AgCl by filtration, excess 2,2′-bipyridine (0.143 g, 2 equiv) was added and the mixture was brought to reflux for a further 3 h. After cooling to room temperature, excess solid NH_4PF_6 was added to the reaction mixture. The volume of the solution was reduced in vacuo to 10 ml and then left overnight at 2 °C. The resultant precipitate was washed with ethanol, diethyl ether, and then dried in vacuo to yield **5**-$(PF_6)_2$ (0.262 g, 68 %). ^{1}H NMR (RT, [D$_6$]acetone): bpy protons: $\delta = 9.44$ (dd, $J = 5.5$, 1.5 Hz, 2H; H^6), 8.90 (ddd, $J = 8$, 1.5, 0.5 Hz, 2H;

H^3), 8.43 (dt, $J=8$, 8, 1.5 Hz, 2H; $H^{4'}$), 7.98 ppm (ddd, $J=8$, 5.5, 1.5 Hz, 2H; H^5); the cyclohexadecane protons have not been assigned but are at $\delta=3.44$ (ddd, $J=12.5$, 7.5, 4 Hz, 4H), 3.29 (ddd, $J=12.5$, 8, 4 Hz, 4H), 3.06 (ddd, $J=13.5$, 6.5, 3 Hz, 4H), 2.69 (dt, $J=10.5$, 10.5, 3 Hz, 4H), 2.55 ppm (m); FAB MS: m/z (%): 699 (100) $[M^+-PF_6]$; elemental analysis calcd (%) for $RuC_{22}H_{32}N_2S_4P_2F_{12}$: C 31.32, H 3.82, N 3.32, S 15.20; found: C 31.02, H 3.97, N 3.54, S 16.12.

$[Ru(L^1)(py)_2](PF_6)_2$, 6-$(PF_6)_2$: To a solution of $[Ru(dmso)Cl(L^1)]PF_6$ (0.3 g, 0.5 mmol) in ethanol/water (1:1, 20 ml), $AgNO_3$ (0.11 g, 1.3 equiv) was added. This mixture was stirred at reflux for 4 hours and the resultant AgCl precipitate was removed by centrifuging. The resultant pale-yellow solution was brought back to reflux and pyridine (1 mL) was added. This mixture was stirred at reflux for 3 h. The solvent was then removed in vacuo and the resultant solid was dissolved in ethanol (25 ml). Excess solid NH_4PF_6 was dissolved into this solution, which was then left overnight at 2 °C. The resultant precipitate was washed with ethanol, diethyl ether, and then dried in vacuo to yield **6**-PF_6 as a bright yellow microcrystalline powder (61 %). H NMR (RT, $[D_6]$DMSO): symmetric isomer: $\delta=8.67$ ($[AM]_2X$; $H^{2,6}$), 8.01 ($[AM]_2X$; H^4) , 7.49 ($[AM]_2X$; $H^{3,5}$), 4.22 (dd, $^2J=14.5$, $^3J=4.5$ Hz; CH_2), 3.66 (dd, $^2J=11$ Hz, $^3J=4.5$ Hz; CH_2), 3.44 (obscured; CH_2), 3.26 ppm (dd, $^2J=11$, $^3J=14$ Hz; CH_2); symmetric isomer: $\delta=8.93$ ($[AM]_2X$; $H^{2,6}$), 8.64 ($[AM]_2X$; $H^{2,6}$), 8.03 ($[AM]_2X$; H^4), 7.96 ($[AM]_2X$; H^4), 7.55 ($[AM]_2X$; $H^{3,5}$), 7.47 ($[AM]_2X$; $H^{3,5}$), 4.55 (dd, $^2J=14$, $^3J=6.5$ Hz; CH_2), 3.97 (dd, $^2J=14$, $^3J=3$ Hz; CH_2), 3.64 (ddd, $^2J=11.5$, $^3J=2$, 3.5 Hz; CH_2), 3.57 (dd, $^2J=11.5$, $^3J=5.5$ Hz; CH_2), 3.46 (dt, $^2J=14$, $^3J=14$, 6 Hz; CH_2), 3.35 (dt, $^2J=14$, $^3J=14$, 3 Hz; CH_2), 3.25 (obscured; CH_2), 2.64 ppm (ddd, $^2J=11.5$, $^3J=13.5$, 5.5 Hz; CH_2); FAB MS: m/z (%): 644 (100) $[M^+-PF_6]$; elemental analysis calcd (%) for $RuC_{18}H_{26}N_2S_4P_2F_{12}$: C 27.37, H 3.29, N 3.55, S 16.22; found: C 27.80, H 3.67, N 3.33, S 15.98.

Crystal structure determinations: Crystals of **4**-$(PF_6)_2$, **5**-$(PF_6)_2$, and **6**-$(PF_6)_2$ were grown by vapor diffusion using acetone and diethyl ether mixtures. Crystallographic data is summarized in Table 1. In all three cases, data was collected at 150 K on a Bruker Smart CCD area detector with Oxford Cryosystems low-temperature system, and complex scattering factors were taken from the program package SHELXTL[13] as implemented on the Viglen Pentium computer. Hydrogen atoms were placed geometrically and refined with a riding model with the isotropic displacement parameter (U_{iso}) constrained to be 1.2 times that of the equivalent displacement parameter (U_{eq}) of the carrier atom.

CCDC 242825–242827 contain the supplementary crystallographic data for this paper. These data can be obtained free of charge from the Cambridge Crystallographic Data Centre via www.ccdc.cam.ac.uk/data_request/cif.

Computational details: Ab initio calculations were performed with the Gaussian 98 software package,[14] running on a PC equipped with a linux operating system (redhat 8.0) at the B3LYP level. The Los Alamos effective core potentials plus double zeta (ζ) of Hay and Wadt (LanL2DZ option of G98)[15] supplemented with an f function ($\zeta=1.235$) for the Ru atom and the Dunning/Huzinaga full double zeta (D95 option of G98)[16] for the remaining atoms, supplemented with a d function in the case of the S atoms ($\zeta=0.532$) were used. The structures of $[Ru([n]aneS_4)(bpy)]^{2+}$ systems (with $n=12$, 14, or 16) in the isomeric forms **a**, **b**, and **c** were fully optimized using gradient methods.

The starting models were generated from X-ray structures, either directly for **1c** or from a structure with the macrocycle in the required conformation. Thus, the remaining starting geometries were obtained by manipulating the atomic coordinates of the structures of related complexes. The comparison between the X-ray structure and the calculated structure for **1c** has been used to check the quality of the method and basis set used.

Acknowledgements

We are grateful for the support of The Royal Society (J.A.T.), The Engineering and Physical Sciences Research Council (EPSRC; M.N. and J.A.T.), and the Erasmus Scheme of the EU (J.A.-M.).

[1] a) C. Creutz, H. Taube, *J. Am. Chem. Soc.* **1969**, *91*, 3988; b) C. Creutz, H. Taube, *J. Am. Chem. Soc.* **1973**, *95*, 1086; c) H. Taube, *Angew. Chem.* **1984**, *96*, 315; *Angew. Chem. Int. Ed. Engl.* **1984**, *23*, 329.

[2] a) C. Creutz, *Prog. Inorg. Chem.* **1983**, *30*, 1; b) R. J. Crutchley, *Adv. Inorg. Chem.* **1994**, *41*, 273; c) W. Kaim, A. Klein, M. Glöckle, *Acc. Chem. Res.* **2000**, *33*, 755; d) B. S. Brunschwig, N. Sutin, *Coord. Chem. Rev.* **1999**, *187*, 233; e) K. D. Demadis, C. M. Hartshorn, T. J. Meyer, *Chem. Rev.* **2001**, *101*, 2655; f) B. S. Brunschwig, C. Creutz, N. Sutin, *Chem. Soc. Rev.* **2002**, *31*, 168.

[3] a) *Mixed Valence Systems: Applications in Chemistry, Physics and Biology* (Ed.: K. Prassides), NATO ASI Series, No. 343, Kluwer Academic, Dordrecht, The Netherlands, **1990**; b) *Electron Transfer in Inorganic, Organic, and Biological Systems* (Eds.: J. R. Bolton, N. Mataga, G. McLendon), *Advances in Chemistry Series*, No. 228, American Chemical Society, Washington DC, **1991**.

[4] a) *Molecular Electronic Devices* (Eds.: F. L. Carter, R. E. Siatkowsky, H. Woltjien), North Holland, Amsterdam, The Netherlands, **1988**; b) M. D. Ward, *Chem. Soc. Rev.* **1995**, *24*, 121; c) V. Balzani, A. Juris, M. Venturi, S. Campagna, S. Serroni, *Chem. Rev.* **1996**, *96*, 759; d) J. P. Launay, *Chem. Soc. Rev.* **2001**, *30*, 386.

[5] a) S. G. Sellmann, L. Zapf, *Angew. Chem.* **1984**, *96*, 799; *Angew. Chem. Int. Ed. Engl.* **1984**, *23*, 807; b) P. J. Blower, S. R. Cooper, *Inorg. Chem.* **1987**, *26*, 2009.

[6] S. Roche, C. Haslam, H. Adams, S. L. Heath, J. A. Thomas, *Chem. Commun.* **1998**, 1429.

[7] a) S. Roche, L. J. Yellowlees, J. A. Thomas, *Chem. Commun.* **1998**, 1429; b) C. S. Araújo, M. G. B. Drew, V. Félix, L. Jack, J. Madureira, M. Newell, S. Roche, T. M. Santos, J. A. Thomas, L. Yellowlees, *Inorg. Chem.* **2002**, *41*, 2260.

[8] N. Shan, S. Vickers, H. Adams, M. D. Ward, J. A. Thomas, *Angew. Chem.* **2004**, *116*, 4028; *Angew. Chem. Int. Ed.* **2004**, *43*, 3938.

[9] a) B. J. Goodfellow, S. M. D. Pacheco, J. Pedrosa de Jesus, V. Felix, M. G. B. Drew, *Polyhedron* **1997**, *16*, 3293; b) T. M. Santos, B. J. Goodfellow, J. Madureira, J. Pedrosa de Jesus, V. Felix, M. G. B. Drew, *New J. Chem.* **1999**, *23*, 1015.

[10] A. J. Blake, G. Reid, M. Schröder, *J. Chem. Soc. Dalton Trans.* **1989**, 1675.

[11] I. P. Evans, A. Spencer, G. Wilkinson, *J. Chem. Soc. Dalton Trans.* **1973**, 204.

[12] E. W. Abel, K. G. Orrell, M. C. Poole, V. Sik, *Polyhedron* **1995**, *14*, 585.

[13] SHELXTL, An integrated system for solving and refining crystal structures from diffraction data (Revision 5.1), Bruker AXS LTD.

[14] Gaussian 98 (Revision A.11), M. J. Frisch, G. W. Trucks, H. B. Schlegel, G. E. Scuseria, M. A. Robb, J. R. Cheeseman, V. G. Zakrzewski, J. A. Montgomery, Jr., R. E. Stratmann, J. C. Burant, S. Dapprich, J. M. Millam, A. D. Daniels, K. N. Kudin, M. C. Strain, O. Farkas, J. Tomasi, V. Barone, M. Cossi, R. Cammi, B. Mennucci, C. Pomelli, C. Adamo, S. Clifford, J. Ochterski, G. A. Petersson, P. Y. Ayala, Q. Cui, K. Morokuma, D. K. Malick, A. D. Rabuck, K. Raghavachari, J. B. Foresman, J. Cioslowski, J. V. Ortiz, B. B. Stefanov, G. Liu, A. Liashenko, P. Piskorz, I. Komaromi, R. Gomperts, R. L. Martin, D. J. Fox, T. Keith, M. A. Al-Laham, C. Y. Peng, A. Nanayakkara, C. Gonzalez, M. Challacombe, P. M. W. Gill, B. G. Johnson, W. Chen, M. W. Wong, J. L. Andres, M. Head-Gordon, E. S. Replogle, J. A. Pople, Gaussian, Inc., Pittsburgh, PA, **1998**.

[15] a) P. J. Hay, W. R. Wadt, *J. Chem. Phys.* **1985**, *82*, 270; b) W. R. Wadt, P. J. Hay, *J. Chem. Phys.* **1985**, *82*, 284; c) P. J. Hay, W. R. Wadt, *J. Chem. Phys.* **1985**, *82*, 299.

[16] T. H. Dunning, Jr., P. J. Hay, in *Modern Theoretical Chemistry*, *Vol. 3* (Ed.: H. F. Schaefer, III), Plenum, New York, **1976**, p. 1.

[17] A. J. Blake, M. A. Halcrow, M. Schroder, *J. Chem. Soc. Dalton Trans.* **1994**, 1463.

[18] A. H. Krotz, L. Y. Kuo, J. K. Barton, *Inorg. Chem.* **1993**, *32*, 5963.

[19] R. M. Silverstein, G. C. Bassler, T. C. Morrill, *Spectrometric Identification of Organic Compounds*, 5th ed., J. Wiley & Sons, New York, p. 197.

[20] N. R. Champness, P. F. Kelley, W. Levason, G. Reid, A. M. Z. Slawin, D. J. Williams, *Inorg. Chem.* **1995**, *34*, 651.
[21] P. F. Kelley, W. Levason, G. Reid, D. J. Williams, *Chem. Commun.* **1993**, 1716.
[22] N. R. Champness, S. R. Jacob, G. Reid, C. S. Frampton, *Inorg. Chem.* **1995**, *34*, 396.
[23] T.-F. Lai, C.-K. Poon, *J. Chem. Soc. Dalton Trans.* **1982**, 1465.
[24] N. W. Alcock, J. C. Cannadine, G. R. Clark, A. F. Hill, *J. Chem. Soc. Dalton Trans.* **1993**, 1131.
[25] A. J. Blake, R. O. Gould, G. Reid, M. Schroder, *J. Organomet. Chem.* **1988**, *356*, 389.
[26] M. Herceg, B. Matkovic, D. Sevdic, D. Matkovic-Cologovic, A. Nagl, *Croat. Chem. Acta* **1984**, *57*, 609.
[27] E. W. Abel, T. P. J. Coston, K. G. Orrell, V. Sik, D. Stephenson, *J. Magn. Reson.* **1986**, *70*, 34.
[28] a) R. Cini, G. Tamasi, S. Defazio, M. Corsini, P. Zanello, L. Messori, G. Marcon, F. Piccioli, P. Orioli, *Inorg. Chem.* **2003**, *42*, 8038; b) V. Felix, T. M. Santos, J. Madureira, F. Mirante, S. Quintal, B. J. Goodfellow, M. G. Santana-Marques, J. Pedrosa de Jesus, M. G. B Drew, M. J. Calhorda, *Inorg. Chim. Acta* **2003**, 356, 335; c) T. Fukuda, E. A. Makarova, E. A. Luk'yanets, N. Kobayashi, *Chem. Eur. J.* **2004**, *10*, 117; X. D. Gong, H. M. Xiao, H. Tian, *Int. J. Quantum Chem.* **2002**, 86, 531.
[29] a) F. H. Allen, *Acta Crystallogr. Sect. B* **2002**, *58*, 380; b) I. J. Bruno, J. C. Cole, P. R. Edginton, M. Kessler, C. F. Macrae, P. McCabe, J. Pearson, R. Taylor, *Acta Crystallogr. Sect. B* **2002**, *58*, 389.

Received: July 7, 2004
Published online: January 26, 2005